



**Renato Paulo dos  
Santos Mendes**

**Modelação numérica da pluma estuarina da Ria de  
Aveiro: estudo preliminar**

**Numerical modeling of the Ria de Aveiro plume: a  
preliminary study**





**Renato Paulo dos  
Santos Mendes**

**Modelação numérica da pluma estuarina da Ria de  
Aveiro: estudo preliminar**

**Numerical modeling of the Ria de Aveiro plume: a  
preliminary study**

Dissertação apresentada à Universidade de Aveiro para cumprimento dos requisitos necessários à obtenção do grau de Mestre em Meteorologia e Oceanografia Física, realizada sob a orientação científica do Prof. Doutor João Miguel Sequeira Dias, Professor Auxiliar do Departamento de Física da Universidade de Aveiro e do Doutor Nuno Alexandre Firmino Vaz, Investigador auxiliar no Centro de Estudos do Ambiente e do Mar (CESAM) da Universidade de Aveiro.

Este trabalho foi desenvolvido no âmbito do projecto DyEPlume: Estuarine Dynamics and Plume Propagation in the Portuguese Coast – Impacts of Climate Change (PTDC/MAR/107939/2008) com o apoio financeiro da Fundação para a Ciência e Tecnologia – FCT.



## **o júri**

presidente

**Prof. Doutor Paulo Manuel Cruz Alves da Silva**  
Professor auxiliar do Departamento de Física da Universidade de Aveiro

**Prof. Doutor João Miguel Sequeira Silva Dias**  
Professor auxiliar do Departamento de Física da Universidade de Aveiro

**Doutor Nuno Alexandre Firmino Vaz**  
Investigador auxiliar do CESAM e Departamento de Física da Universidade de Aveiro

**Doutor Paulo Miguel Chambel Filipe Lopes Teles Leitão**  
Consultor, Hidromod, Modelação em Engenharia Lda.



## **acknowledgements**

I would like to thank many people who helped, supported and participated actively to carry on my study.

To my supervisor, Prof. Doutor João Miguel Dias, for his scientific supervision but also for the patience and trust in my work.

To my “lab supervisor” Doutor Nuno Alexandre Firmino Vaz for his patience to help me in the Mohid introduction, to solve several problems at any time and for constant brainstorming along this study.

I also wish to thank to Eng. Marco Almeida and Eng. Fernando Ribeiro from ARH (Hydrographic Regional Administration) – Coimbra to provide actual bathymetric data from Ria de Aveiro lagoon and for the attention always shown throughout my visit to Coimbra and later emails.

Thanks to Prof. Doutor João Thadeu Menezes, from UNIVALI and to Prof. Doutor Fernando Almeida, from UA, for their help in the ArcGis® software handling.

Thanks to all my friends and colleagues at the “Laboratório de Atmosfera” for the exchange of knowledge and ideas throughout my work.

Thanks to my all friends from UA and UNIVALI (Brazil) but especially to my “old friends”.

To my incredible family who was always present in my studies and in my life at every moment.

Thanks Ju for your help, support and comprehension in these last months.



## Palavras-chave

Pluma estuarina; Modelo Numérico; Landsat7; Caudal fluvial

## Resumo

A Ria de Aveiro é um dos principais sistemas estuarinos de águas pouco profundas de Portugal. Situa-se na costa Norte de Portugal e está sujeita, dentro da sua complexa rede de canais e zonas intertidais, a um *stress* elevado (natural e o antropogénico).

Realizaram-se vários estudos de modelação numérica na Ria de Aveiro, mas nenhum deles teve como objectivo o estudo da dinâmica da pluma estuarina da laguna para o Oceano Atlântico. Estes fluxos estuarinos de águas menos densas penetram nas águas oceânicas (mais salinas), produzindo uma circulação na camada superficial para o largo durante as situações de vazante. As plumas estuarinas caracterizam-se normalmente por apresentarem uma estrutura côncava radial, podendo a sua forma variar devido a diversos factores: diferenças entre propriedades da água do oceano e da descarga estuarina; variações batimétricas; e factores meteorológicos, em particular a direcção e intensidade dos ventos.

Este trabalho tem como principal objectivo um estudo preliminar de modelação numérica da pluma estuarina da Ria de Aveiro, assim como uma avaliação qualitativa desta para condições extremas (máxima e mínimas) e típicas de descarga fluvial, para todas as fontes de água doce da Ria, para o mês de Janeiro.

Neste âmbito foi implementado para a Ria de Aveiro o modelo numérico de volumes finitos Mohid em modo 2D, de forma quantificar o fluxo (e as suas propriedades) que a laguna injecta no oceano. O modelo foi calibrado e validado (processos hidrodinâmicos e de transporte), tendo-se obtido valores de erro de *RMS* e *Skill* que comprovam a precisão das suas previsões numéricas. Posteriormente, foram simulados os três diferentes cenários de caudal fluvial estabelecidos.

Após este processo, e seguindo a metodologia de utilização de modelos aninhados, foram criados outros dois domínios costeiros. O primeiro (no modo 2D) abrange toda a Península Ibérica e zonas envolventes, com uma resolução variável ( $0.02^{\circ}$ - $0.04^{\circ}$ ), sendo forçado por um modelo global de maré nas suas fronteiras laterais. O segundo (no modo 3D), de maior resolução ( $0.01^{\circ}$ ), localiza-se entre a Figueira da Foz e Caminha. A descarga horária calculada por simulação utilizado o modelo da Ria de Aveiro é imposta neste segundo domínio, na localização da embocadura, possibilitando o estudo da dinâmica da Ria de Aveiro.

Os resultados das simulações para a zona costeira adjacente à Ria de Aveiro mostram padrões semelhantes comparativamente a imagens de satélite obtidas pelo sensor TM-Landsat7 à superfície, para um cenário de intenso caudal fluvial. Nas simulações com caudais máximos a pluma expande-se até cerca de 25 km da embocadura da laguna, apresentando uma forma côncava em frente à mesma. A pluma é posteriormente advectada para a direita (efeito de Coriolis) e após o estabelecimento do equilíbrio geostrófico é transportada para Norte. Para os caudais típicos os resultados têm padrões semelhantes, mas menos acentuados. No caso das simulações para o caudal mínimo a pluma é inexistente. Neste cenário, as diferenças de salinidade ( $<0.5$  psu) são mínimas e são os gradientes térmicos que tendem a controlar a formação da pluma.

Esta abordagem poderá ser um ponto de partida para novos estudos e melhoramentos na monitorização da dinâmica da pluma da Ria de Aveiro.



## keywords

Estuarine plume; Numerical model; Landsat7; River Discharges

## Abstract

The Ria de Aveiro is one of the largest shallow water estuarine systems of Portugal. It is located on the northern coast of Portugal and it is characterized by a large number of narrow channels and intertidal areas, subject to an enormous natural and anthropic stress. Therefore, it becomes essential the numerical study of its hydrodynamics.

In recent years, several studies regarding numerical modeling of the lagoon have been performed, but none of them had its focus on the dynamics of the estuarine plume of the lagoon to the Atlantic Ocean. This buoyant plume injects less dense water which penetrates onto the coastal zone. Then, it is generated an offshore movement in the surface layer during the ebbing.

The structure of the estuarine plume is usually characterized by a buoyant bulge, propagating radially. Their shape may vary due to several factors: differences in the ocean and estuarine discharge water properties; bathymetric variations; and meteorological factors, in particular the wind direction and intensity.

The main objective of this study is to perform a preliminary study of the Ria de Aveiro estuarine plume, as well as its qualitative assessment during extreme river discharges conditions (maximum and minimum) and a typical value to January.

The baroclinic finite volume numerical model, Mohid, was implemented to the Ria de Aveiro in a 2D mode, in order to quantify the flow (and its properties) that the lagoon injects into the ocean. The model was calibrated and validated (hydrodynamic and transport processes), and the RMS errors and Skill values reflect the good performance of the model. After the three different river discharges scenarios were simulated.

Then, based on the nested models methodology were created two other coastal domains. The first (2D mode) covers the entire Iberian Peninsula and surrounding areas, with a variable resolution (0.02°-0.04°), and it was forced by a global tidal model in its lateral boundaries. The second (3D mode), with more resolution (0.01°) is located between Figueira da Foz and Caminha, and includes the coastal area of the plume propagation. The hourly lagoon discharge, previously calculated through the model runs of Ria de Aveiro, was imposed in the lagoon mouth location, in order to allow the study of the estuarine plume dynamics.

The forecast results for the coastal zone adjacent to Ria de Aveiro show similar patterns comparing to satellite images obtained by the TM sensor-Landsat7, at the surface, to a day of intense river inflow. In the highest flow simulation, the plume expands to about 25 km, creating a bulge in front of the lagoon mouth. Then, it is advected to the right (Coriolis effect) and after the establishment of the geostrophic balance is extended along the northern coast. The typical inflow results have similar patterns, but less pronounced. The simulations for the minimum inflow rate show that the plume is almost nonexistent. In this scenario, the salinity differences are minimal (<0.5 psu) and the thermal gradients tend to control the estuarine plume establishment.

This approach could be a starting point for further studies and improvements in the monitoring of the dynamics of Ria de Aveiro plume.



**Contents**

<b>Acknowledgements</b>	<b>i</b>
<b>Resumo</b>	<b>iii</b>
<b>Abstract</b>	<b>v</b>

**LIST OF FIGURES ..... IX**

**LIST OF TABLES ..... XI**

<b>1 INTRODUCTION .....</b>	<b>1</b>
1.1 MOTIVATIONS AND AIMS.....	1
1.2 STATE OF THE ART .....	2
1.2.1 Mohid .....	2
1.2.2 Estuarine Plume.....	3
<b>2 STUDY AREA .....</b>	<b>5</b>
2.1 GENERAL DESCRIPTION .....	5
2.2 PHYSICAL DESCRIPTION.....	6
<b>3 ESTUARINE PLUMES .....</b>	<b>7</b>
3.1 INTRODUCTION.....	7
3.2 NEAR AND FAR-FIELD PLUME.....	7
3.3 SURFACE ADVECTED PLUMES .....	8
<b>4 NUMERICAL MODEL: MOHID .....</b>	<b>11</b>
4.1 THE NUMERICAL MODEL EQUATIONS .....	11
4.2 DISCRETIZATION .....	12
4.3 BOUNDARY CONDITIONS .....	12
4.4 SURFACE HEAT FLUXES PARAMETERIZATIONS .....	14
<b>5 HYDRODYNAMIC MODEL IMPLEMENTATION TO THE RIA DE AVEIRO .....</b>	<b>17</b>
5.1 NUMERICAL GRID CONSTRUCTION .....	17
5.2 HYDRODYNAMIC MODEL CALIBRATION.....	20
5.2.1 Results .....	20
5.3 HYDRODYNAMIC MODEL VALIDATION .....	23
5.3.1 Results .....	23
<b>6 CALIBRATION AND VALIDATION OF THE SALT AND HEAT TRANSPORT MODEL.....</b>	<b>27</b>
6.1 INTRODUCTION.....	27
6.2 CALIBRATION .....	27

---

6.2.1	Data set and Methods .....	27
6.2.2	Results .....	28
6.3	VALIDATION.....	29
6.3.1	Results .....	29
<b>7</b>	<b>ESTUARINE PLUME SIMULATION .....</b>	<b>33</b>
7.1	THE RIA DE AVEIRO RUNOFF.....	33
7.2	NESTED COASTAL MODEL .....	34
7.3	RESULTS AND DISCUSSION.....	35
<b>8</b>	<b>CONCLUSIONS AND FUTURE IMPROVEMENTS .....</b>	<b>43</b>
	<b>REFERENCES.....</b>	<b>45</b>

## List of Figures

2.1: The Ria de Aveiro lagoon. ....	5
3.1: An idealized near-field plume simulation. The upper panel shows a gray-scale of surface salinity, the lower panel shows a cross-section of salinity down the center of the plume. The freshwater flow is initiated at t=0 hours (a) t=1.0 hours; b) t=2.5 hours; c) t=5.0 hours; and d) t=6.0 hours) [Robert D. Hetland: <a href="http://pong.tamu.edu/~rob/plume/near_movie.mov">http://pong.tamu.edu/~rob/plume/near_movie.mov</a> ]. ....	8
3.2: Scheme of a surface-advected plume [Yankovsky and Chapman, 1997]. ....	9
3.3: Regions of various plume types based on the Yankovsky and Chapman [1997] theory. ....	10
4.1: Conditions for a cell to be considered uncovered (moving boundaries) [Leitão, 2003] ....	14
5.1: A) Map of depth databases used in numerical bathymetry actualization. B) Numerical grid of the Ria de Aveiro lagoon. ....	18
5.2: A) Relative difference of $M_2$ amplitude between grid 1 (data from 2 m above local datum) and grid 2 (data from 7 m above local datum). B) Phase difference of $M_2$ between grid 1 and grid 2; C) Relative difference of $S_2$ amplitude between grid 1 and grid 2; D) Phase difference of $S_2$ between grid 1 and grid 2. ....	19
5.3: Comparison between SSE time series for stations A, B, C, D, E, F, G, H, I, J, and K used in the hydrodynamic calibration procedure (● red: data; black solid line: model). ....	21
5.4: Comparison between model predicted and observed amplitude and phase for the major semi-diurnal and diurnal constituents ( $M_2$ – 12.42 h; $S_2$ – 12 h; $N_2$ – 12.9 h; $K_1$ – 23.93 h; $O_1$ – 25.82 h) and for the shallow water overtide of the principal lunar constituent, $M_4$ (6.21 h). The black and white bars represent the observed and predicted values, respectively. ....	23
5.5: Comparison between SSE time series for stations B, H, K, J, L, M, N, O, P, and Q, used in the hydrodynamic validation procedure (● red: data; black solid line: model). ....	25
5.6: Comparison between time series of along flow direction for stations B, H, K, J, L, M, N, O, P, and Q, used in the hydrodynamic validation procedure (● red: data; black solid line: model). ....	25
6.1: Comparison between salinity time series for the stations used during the calibration procedure. (● red: data; black solid line: model). ....	28
6.2: Comparison between water temperature time series for the stations used during the calibration procedure. (● red: data; black solid line: model). ....	29
6.3: Comparison between salinity time series for the stations used during validation procedure. (● red: data; black solid line: model). ....	30
6.4: Comparison between water temperature time series for the stations used during validation procedure. (● red: data; black solid line: model). ....	31
7.1: Location of the transversal section used to compute the Ria de Aveiro lagoon outflow. ....	34
7.2: Location of the D1 and D2 domains. ....	35
7.3: Average discharge scenario predictions during January. A) Time series of discharge through the lagoon mouth (red line means the limit between the positive (into the lagoon) and negative (into the ocean) outflow; the green points represent the time for model outputs; 0 is the simulation initial time). B) Salinity horizontal patterns and velocity fields for each time step – 1, 2, 3, and 4. C) Salinity cross-section perpendicular to Ria de Aveiro mouth in each time step – 1, 2, 3, and 4 (salinity values above 36 psu are shown in white). ....	38

- 
- 7.4: Extreme maximum discharge scenario predictions during January. A) Time series of discharge through the lagoon mouth (red line means the limit between the positive (into the lagoon) and negative (into the ocean) outflow; the green points represent the time for model outputs; 0 is the simulation initial time). B) Salinity horizontal patterns and velocity fields for each time step – 1, 2, 3, and 4. C) Salinity cross-section perpendicular to Ria de Aveiro mouth in each time step – 1, 2, 3, and 4 (salinity values above 36 psu are shown in white). ..... 39
- 7.5: Extreme minimum discharge scenario predictions during January. A) Time series of discharge through the lagoon mouth (red line means the limit between the positive (into the lagoon) and negative (into the ocean) outflow; the green points represent the time for model outputs; 0 is the simulation initial time). B) Salinity horizontal patterns and velocity fields for each time step – 1, 2, 3, and 4. C) Salinity cross-section perpendicular to Ria de Aveiro mouth in each time step – 1, 2, 3, and 4 (salinity values above 36 psu are shown in white). ..... 40
- 7.6: Landsat7-TM observations in 18th December 2006. A) Composite of RGB bands of TM sensor (visible image). B) Thermal Infrared Band of TM sensor. C) Reclassification of Thermal Infrared Band to distinguished the surface ocean waters with the same thermal characteristics as the lagoon mouth waters. D) Tidal prediction for Aveiro by neptuno.fis.ua [Marta-Almeida and Dubert, 2006] (11:04 was the time detection); E) Meteorological conditions computed for Aveiro by windguru.cz. .... 41

## List of Tables

7.1: River discharges values used in the Ria de Aveiro outflow simulation.....	34
--	----



# 1 Introduction

## 1.1 Motivations and aims

Estuaries and the adjacent shelf are very complex and highly dynamic regions subject to enormous natural and anthropic stress. The Ria de Aveiro lagoon is an evident example of this, since it is inserted in heavily populated region and in the vicinity of important commercial and fishing ports.

The estuarine dynamics is determined by a complex interaction between tide, waves, wind and buoyancy inputs from rivers. Usually, the investigation of coastal processes is been performed independently for estuaries and the adjacent coast. This work seeks a wider and integrated assessment of how changes in the major forcing factors affect the hydrodynamic and, in the future, biogeochemical response of coupled estuarine-coastal systems.

It is essential to note that estuaries impact the adjacent shelf through the estuarine plumes, affecting the physical and biogeochemical features of these coastal regions. According to Orton and Jay [2005], major rivers inject freshwater onto the adjacent shelf where mixing of these river plumes takes place, affecting the transport and transformation of dissolved and particulate materials at the coastal margin. Therefore, extreme events of river discharge associated to torrential rain episodes, that are becoming more frequent in southern Europe [IPCC, 2007] will affect the balance of these coupled systems [Choi and Wilkin, 2006; Guo and Valle-Levinson, 2007; Lihan *et al.*, 2008].

According to Mestres *et al.* [2007], estuarine plumes are relevant to many aspects of the coastal environment, from shelf circulation [Weaver and Hsieh, 1987] to biogeochemical processes [Naudin *et al.*, 2001; Le Pape *et al.*, 2003; Chen and Gardner, 2004], including the enhancement of biological production due to river borne nutrients, the hampering of primary production because of the reduction in light penetration [Froidefond *et al.*, 1998] and other processes related to coastal pollution, larval transport and sediment or geochemical transport across the shelf [Jouanneau and Latouche, 1982; Fichez *et al.*, 1992; Morris *et al.*, 1995; Blanton *et al.*, 1997]. These factors will influence, directly or indirectly, various socio-economic aspects that affect the entire population in areas near the lagoon/river mouth.

In recent years, various studies about the Ria de Aveiro have been performed with several numerical models, such as: MOHID [Vaz, *et al.*, 2007; 2009a], ELCIRC [Picado *et al.*, 2010], and SIMSYS2D [Dias, 2001; Dias and Lopes, 2006; Mendes *et al.*, 2009]. Nevertheless, no studies regarding the Ria de Aveiro estuarine plume were carried out.

Vaz [2007] presents a study which had as the main objective the research of the Espinheiro channel's thermohaline dynamics as a function of two major forcings: tides and river inflow using field experiments and numerical modelling simulations. The Mohid numerical model was then implemented using a numerical grid of  $40 \times 40$  m for the central area of the lagoon, and then used to study the channels hydrography.

Although this intensive study of the Ria de Aveiro hydrodynamics, this model configuration is not suitable to be used in this work since it has some limitations. A future goal of this work will be the coupling of other Mohid modules, such as the biogeochemical model (Life, Mateus, 2006). As stated before, the study of estuarine plumes include other scientific areas beyond the physical dynamics. The numerical grid bathymetry used by Vaz [2007] turns the computational effort too

high to allow the coupling with ecological modules. Thus, it became necessary to build a lower resolution grid ( $100 \times 100$  m).

The main objective of this study is carrying out a preliminary and qualitative analysis of the Ria de Aveiro estuarine plume behavior under some extreme and typical rivers discharges scenarios during January. Combined with this principal objective, there are other specific objectives such as: update and construct a numerical grid for the Ria de Aveiro using the most recent bathymetry data set; calibrate and validate the numerical model Mohid (hydrodynamic and transport modules in a 2D mode) for the Ria de Aveiro lagoon with a numerical grid with 100 m of cell width; implement a nested methodology to couple the Ria de Aveiro model with coastal zone model; and build thematic maps of the possible Ria de Aveiro estuarine plumes observations from remote sensing data from TM sensor of the LANDSAT7 satellite and qualitatively compare with the modeling results.

## 1.2 State of the Art

### 1.2.1 Mohid

In this work is used the numerical model Mohid – Water Modelling System. Mohid is a 3D baroclinic finite volume marine model, designed for coastal and estuarine shallow water applications, like the study of Ria de Aveiro dynamics. The model is under continuous development at the Instituto Superior Técnico (Universidade Técnica de Lisboa) [Santos, 1995; Martins *et al.*, 2001; Leitão, 2003; Leitão *et al.*, 2005]. Mohid is constituted by several other modules like an Eulerian/Lagrangian transport module, or a sediments module. The hydrodynamic model may be used to force biogeochemical models [Mateus, 2006]. A complete description of the model physics can be found in Leitão [2003] and Leitão *et al.* [2005].

Since its creation, Mohid has been applied to different coastal and estuarine areas, showing its capability to simulate complex flows features. In Portugal, several estuarine systems have been studied: Douro [Silva, 1996] and Mondego rivers [Saraiva, *et al.*, 2007] (river mouths); Ria de Aveiro [Trancoso *et al.*, 2005; Vaz *et al.*, 2005, 2007, 2009a], Óbidos lagoon [Santos *et al.*, 2006; Malhadas *et al.*, 2009] and Ria Formosa [Silva *et al.*, 2002] (coastal lagoons); Tagus [Braunschweig *et al.*, 2003; Vaz *et al.*, 2009b], Sado [Martins *et al.*, 2001], and Guadiana estuaries [Saraiva, *et al.*, 2007] (coastal plain estuaries). Furthermore, Mohid has been implemented in other parts of Iberian Peninsula: for example in the Galician Rias (Ria de Pontevedra [Villarreal *et al.*, 2002] and Ria de Vigo [Taboada *et al.*, 1998; Montero, 1999]).

Besides these, other studies were performed in open sea: on the Iberian Coast, including the Portuguese coastal circulation [Coelho *et al.*, 2002], slope Cantabrian current [Villarreal *et al.*, 2004], and Algarve coastal circulation [Leitão *et al.*, 2005], and on the North Sea [Bernardes, 2007].

All this extensive number of studies in several coastal environments, with different resolutions and the ability to future incorporation of other modules (such as biogeochemical) allow to show that the numerical model, Mohid, has the total capabilities to simulate the dynamics of the Ria de Aveiro estuarine plume.

### 1.2.2 Estuarine Plume

There is an extensive literature on buoyant plumes in shelf water, including observational, laboratory model, and mathematical (including numerical) model studies. Garvine [1987] developed a classic model of plume dynamics which balance the buoyancy force with the Coriolis force that causes the river outflow to turn right in the northern hemisphere. These buoyant outflows may also contain a bulge in its vicinity. Yankovsky and Chapman [1997] incorporated a bulge in a steady-state model and distinguished the surface-advected plume from bottom-advected plume. Recent modeling and laboratory studies of buoyant outflows provide a more detailed characterization of bulge structure [Fong and Gyer, 2001; Avicola and Huq, 2003; Horner-Devine *et al.*, 2006]. Other studies show that local wind forcing significantly affects the dispersal of river plume [Whitney and Garvine, 2005; Choi and Wilkin, 2006]. Tidal effects on estuarine plume are also study in recent times by Guo and Valle-Levinson [2007].

In Portugal, they were found several biological studies including some research about the interaction of the coastal ocean with estuarine plumes dynamic. Vaz *et al.* [2009b] studied the Tagus estuarine plume dynamics induced by wind and freshwater discharges. In this work a three-dimensional ocean circulation model (Mohid) with realistic high and low frequency forcing is used to get insight on how the Tagus River plume responds to wind and freshwater discharge during winter.



## 2 Study area

### 2.1 General Description

Located on the northern coast of Portugal ( $40^{\circ}38' N$ ,  $8^{\circ}45' W$ ), the Ria de Aveiro (Figure 2.1) is a shallow water lagoon – the most extensive in Portugal [Teixeira, 1994] – separated from the Atlantic Ocean by a sand dune barrier. It has an irregular geometry, and its only connection with Atlantic Ocean is through an artificial channel (Barra de Aveiro), opened in the beginning of 19<sup>th</sup> century [Dias, 2001]. It reaches a maximum width of 8.5 km and extends for over 45 km. Four main branches radiate from this sea entrance: Mira, São Jacinto, Ílhavo and Espinheiro channels. The Mira channel is an elongated shallow arm, with 29 km length. S. Jacinto channel is about 29 km long, and Ílhavo and Espinheiro are 15 and 17 km, respectively [Dias, 2001].

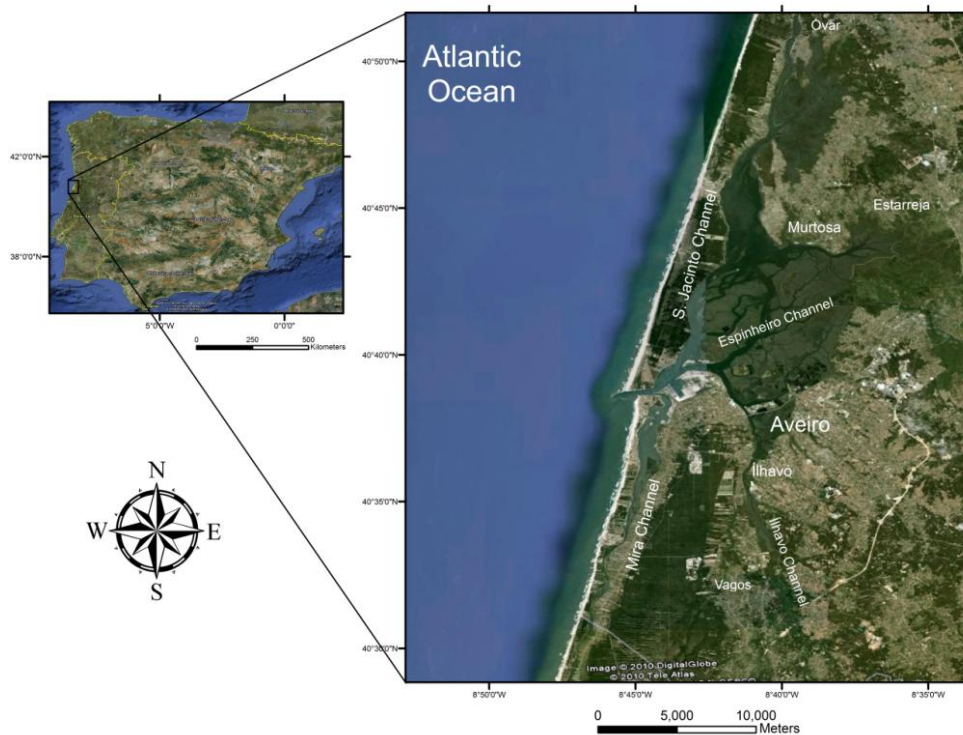


**Figure 2.1: The Ria de Aveiro lagoon.**

It provides natural conditions for harbour, and navigation facilities and it is also a place of discharge of domestic and industrial wastes. It offers good conditions for agricultural development along its borders and for the set up of a large number of small and medium industries.

There are a considerable number of semi-professional and part-time fishermen who economically depend on the productivity of the lagoon waters. Meanwhile, an increasing number of recovered pans for aquaculture purposes imply that in near future this activity may become economically promising. The harbour reveals a strong development in recent years due to the increasing number of industries in Aveiro region. Due to the development of some of the referred activities, the lagoon is being subjected to considerable pollution stress. For example, the most

enclosed and remote arms of the lagoon show evident signs of advanced eutrophication, some communities and animal species have survival problems, there is microbiological contamination from large discharge of untreated sewage and there is industrial pollution. The recent progress of saline intrusion is another important problem, responsible for significant saline stress in the low-lying lands of Baixo Vouga. Once flooded by sea water, previously fertile lands are unsuitable for growing crops for several years because of the saline deposits which remain after the floods have receded [Frazão *et al.*, 2010].

## 2.2 Physical Description

The Ria de Aveiro presents a significant variable area due to the large tidal influence on its hydrodynamics. In spring tides it reaches a maximum area of 83 km<sup>2</sup> at high tide, which reduces to a minimum of 66 km<sup>2</sup> at low tide [Dias, 2001]. The system is characterized by extensive intertidal areas, essentially mudflats, salt marsh and old saltpans. The average depth of the Ria de Aveiro is 1 m (relative to the local datum), but the navigation channels close to its mouth and the areas contiguous to the ports are deeper, because of the constant dredging operations to allow the access of large ships to the harbor.

The lagoon is mesotidal, presenting a tidal amplitude at the inlet of 0.6 m in neap tides and 3.2 m in spring tides - average 2 m [Dias *et al.*, 2000]. Moreover, the semidiurnal tides are the major factor influencing the hydrodynamics of the lagoon [Dias *et al.*, 2000]. The  $M_2$  and  $S_2$  constituents represent 88% and 10% of total tidal energy, respectively [Dias, 2001]. The  $M_2$  constituent presents, at lagoon mouth, an amplitude of  $\sim 0.96$  m and a phase of  $\sim 78^\circ$ . The  $S_2$  shows an amplitude of  $\sim 0.36$  m and a phase of  $\sim 80^\circ$ , in line with harmonic analysis of Sea Surface Elevation (SSE) measured in 1987 by Hydrographic Institute of Portuguese Navy and presented by Vaz *et al.* [2007]. According to Araújo, *et al.* [2008], the Ria de Aveiro lagoon show an average increase of 0.245 m in  $M_2$  amplitude and  $17.4^\circ$  decrease in phase, over 16 years (1987 – 2004). Its estimated tidal prism is  $136.7 \times 10^6$  m<sup>3</sup>, at lagoon mouth, for maximum spring tide and  $34.9 \times 10^6$  m<sup>3</sup> for maximum neap tide [Dias, 2001] and, in almost all situations it is very large compared with estimated total freshwater input. According with Moreira *et al.* [1993] it is about  $1.8 \times 10^6$  m<sup>3</sup> during a tidal cycle.

In extreme situations of wind and freshwater forcing, these can also influence the Ria de Aveiro hydrodynamics. There are several rivers discharging along all the surrounding area of Ria de Aveiro. The most important, considering the mean river inflow rate, are the Vouga ( $\sim 50$  m<sup>3</sup>s<sup>-1</sup>), Antuã ( $\sim 5$  m<sup>3</sup>s<sup>-1</sup>), and Boco (maximum value of  $0.47$  m<sup>3</sup>s<sup>-1</sup>). Besides these, there are also some other smaller rivers that discharge into the northern channels (Caster, Gonde and Fontela) and to the Mira Channel. In spite of the complex interaction between its morphology, tidal effects and its tributary river drainage seasonal variability, the Ria de Aveiro can nonetheless be considered a vertically homogeneous estuarine environment during most of the year. During an exceptional situation of strong freshwater flows, the lagoon is weakly stratified [Dias *et al.*, 1999].

## 3 Estuarine Plumes

### 3.1 Introduction

River or estuaries discharge into the coastal ocean represent a major link between terrestrial and marine systems. Furthermore, the majority of the world human population is located around coastal and estuarine zones. Thus, those discharges are an important anthropogenic pollution pathway to the ocean. These flows are fewer dense than the saline ocean water and this difference produce a buoyancy force that drives the plume circulation. This buoyant outflow is advected onto the near shelf during the ebbing and when it is spread over more saline coastal water, vertical mixing occurs (including a stronger seaward transport). In compensation, the lower layer tends to flow landward, onto the estuary.

The structure of the estuarine plume, as it is expected in the Ria de Aveiro, may take a variety of shapes depending on the ambient flow, bottom topography, inflow properties, and wind forcing. For example, the interaction between the buoyant surface and the bottom, among other things, determines the extent of the sediment transport near the bottom as well as the stratification and dynamics of the plume. Chao [1988] and Marsaleix *et al.* [1998] show that the topography of the continental shelf plays an important role in the estuarine plume evolution. The effect of seaward bottom slope limits the offshore development of the bulge by increasing the anticyclonic vorticity to the orographic lifting of undercurrent. For example, the presence of a canyon in front of the estuarine mouth reinforces the barotropic circulation with the generation of coastally trapped waves [Weaver and Hsieh, 1987].

Some studies on the northern Portuguese and Galician shelf highlight important characteristics of the system response to wind events and river runoff. Santos *et al.* [2004] and Ribeiro *et al.* [2005] reveal the influence of the buoyancy from the rivers, which combine with a warmer and saltier poleward current, on the shelf/slope circulation during the autumn. Otero *et al.* [2010] reveal in their study the role of the alongshore winds in the confinement – downwelling favourable – or export of the buoyant outflow – upwelling favourable.

The buoyant outflows may also contain a bulge-like region in the vicinity of the outflow, and the cross-shelf extent of these bulges can be several times the width of the downstream coastal current [Chant *et al.*, 2008].

### 3.2 Near and Far-field Plume

Hetland [2005] decomposes the system estuary or river plume into three components: the estuary; the near-field and far-field plumes. Essentially, the estuary and the near-field plume are characterized by powerful mixing of fresh and salt water. The near-field plume also can be characterized by supercritical Froude number, enhanced mixing, and rapid water mass modification. The supercritical flow is initiated by topographic control at the estuary mouth and results in intense mixing and high flow speeds that are typically not present in the coastal ocean which it is controlled by variations in river flow and tides. The far-field plume refers to the region outside the influence of the river runoff, and it is mainly modulated by the wind forcing [Halverson and Pawlowicz, 2008]. Figure 3.1 shows an idealized numerical simulation of a near-field plume.

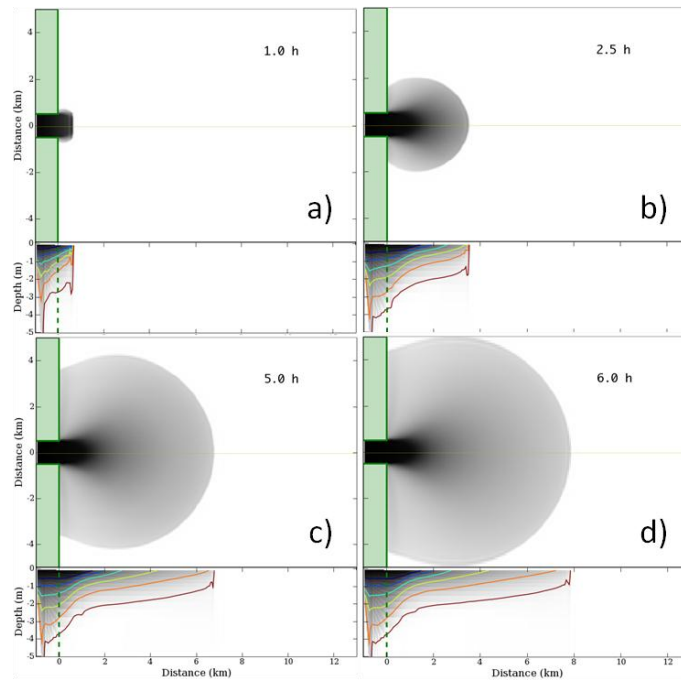


**Figure 3.1: An idealized near-field plume simulation. The upper panel shows a gray-scale of surface salinity, the lower panel shows a cross-section of salinity down the center of the plume. The freshwater flow is initiated at t=0 hours (a) t=1.0 hours; b) t=2.5 hours; c) t=5.0 hours; and d) t=6.0 hours) [Robert D. Hetland: [http://pong.tamu.edu/~rob/plume/near\\_movie.mov](http://pong.tamu.edu/~rob/plume/near_movie.mov)].**

### 3.3 Surface advected plumes

Yankovksy and Chapman [1997] developed a simple theory that predicts the vertical structure and offshore spreading of a localized buoyant inflow onto a continental shelf. The theory is based on two competing mechanisms that move the buoyant fluid offshore: 1- the radial spread of lighter water over the ambient water, being deflected by the Coriolis force and producing an anticyclonic cyclostrophic plume, and 2- offshore transport of buoyant water in the frictional bottom boundary layer that moves the entire plume offshore while maintaining contact with the bottom. Considering the Hetland [2005] classification, the Ria de Aveiro estuarine plume can be defined as a near-field plume. Consequently, being classified as a near-field plume it is also a surface-advected plume. Thus, in this work only the surface-advected plume theory will be described in detail.

They developed a formulation to quantify the distance ( $y_s$ ) that the plume moves offshore in an idealized model, without any exterior forcing except the inflow value:

$$y_s = \frac{2(3g'h_0 + v_i^2)}{(2g'h_0 + v_i^2)^{1/2}f} \quad (3.1)$$

where  $g'$  is the reduced gravity,  $h_0$  is the inflow depth,  $v_i$  is a constant and spatially uniform velocity inflow, and  $f$  is the Coriolis parameter.

They formulated the computation of another important variable in the estuarine plume dynamics:  $h_b$  is considered the depth which the plume remains attached to the bottom:

$$h_b = \left( \frac{2Lv_i h_0 f}{g'} \right)^{1/2} \quad (3.2)$$

$L$  is the inflow width.

Detailed explanations about the base of these theoretical calculations may be found in Yankovksy and Chapman [1997]. It's possible to identify three scenarios from these values:

- 1-  $h_b > h_0$ , and  $y_b$  is offshore of  $y_s$ : A **bottom-advected plume** is generated.
- 2-  $h_b < h_0$ : The predicted equilibrium depth for the bottom-advected plume is shallower than the depth of the buoyant inflow, so bottom boundary layer have no influence. A **surface-advected plume** is generated (Figure 3.2). In this case  $y_b = 0$ .
- 3-  $h_b > h_0$ ,  $h_b$  is shoreward of  $y_s$  (i.e.  $0 < y_b < y_s$ ): An **intermediate plume** is generated.

If the values of  $h_b$  indicate that it is a surface-advected plume it is interesting to take into account the  $v_i$  magnitude. Two limits are important: 1) if the  $v_i^2 \ll g'h_0$ ,  $y_s = 4.24R_{di}$ . Where  $R_{di}$  may be referred to as the barotropic Rossby radius of the buoyant inflow and it is equal to:

$$R_{di} = \frac{(g'h_0)^{1/2}}{f} \quad (3.3)$$

These are the cases of weak buoyant flows or large density differences. 2) In the limit of strong inflow or small density difference  $v_i^2 \gg g'h_0$ , then the  $y_s = \frac{2v_i}{f}$ , and inflows turns in an inertial circle.

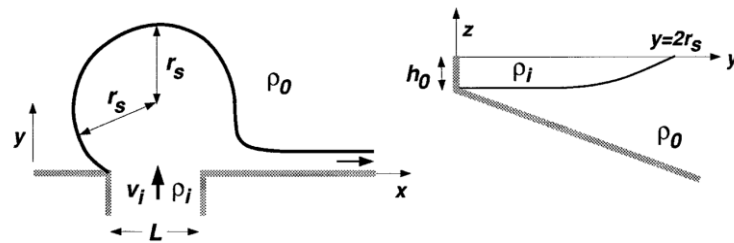


Figure 3.2: Scheme of a surface-advected plume [Yankovksy and Chapman, 1997].

Another point of view based on the two nondimensional parameters simplifies the interpretation referred before. Considering the definitions of Burger ( $S$ ) and Rossby ( $R_0$ ) numbers:

$$S = \frac{(g'h_0)^{1/2}}{fL} \quad (3.4)$$

$$R_0 = \frac{v_i}{fL} \quad (3.5)$$

The Rossby number is a measure of nonlinear advection of momentum through the coast or, more specifically, the rate of inflow. While the Burger number is a measure of the influence of

buoyancy. Yankovsky and Chapman [1997], according to these terms, built a diagram (Figure 3.3) which turn easier the identification of each type of estuarine or river plume:

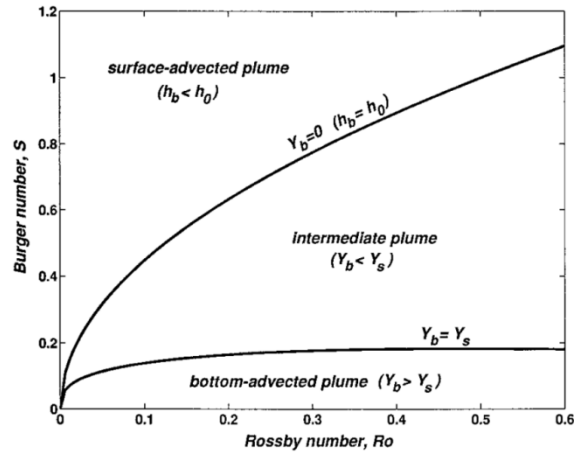


Figure 3.3: Regions of various plume types based on the Yankovsky and Chapman [1997] theory.

## 4 Numerical Model: Mohid

### 4.1 The Numerical Model Equations

The numerical model Mohid solves the three-dimensional incompressible primitive equations. Hydrostatic equilibrium is assumed as well as the Boussinesq and Reynolds approximations. The hydrostatic approximation gives:

$$\rho(z) = \rho_{atm} + \rho_0 g(\eta - z) + \int_{-h}^{\eta} \rho' dz \quad (4.1)$$

Equation (4.1) relates pressure at any depth with the atmospheric pressure at the sea surface, the sea level and pressure anomaly integrated between that level and the surface. Using the Boussinesq approximation it is possible to describe the total pressure gradient as the sum of the gradients of the atmospheric pressure, the sea surface elevation (barotropic pressure gradient) and the density distribution (baroclinic pressure gradient):

$$\frac{\partial p}{\partial x_i} = \frac{\partial p_{atm}}{\partial x_i} - g\rho_0 \frac{\partial \eta}{\partial x_i} - g \int_z^{\eta} \frac{\partial \rho'}{\partial x_i} dz \quad (4.2)$$

This decomposition is substituted in the 3D incompressible primitive equations and yields to the mass momentum equation (4.3):

$$\begin{aligned} \frac{\partial u_i}{\partial t} + \frac{\partial (u_i u_j)}{\partial x_j} = & -\frac{1}{\rho_0} \frac{\partial p_{atm}}{\partial x_i} - g \frac{\rho(\eta)}{\rho_0} \frac{\partial \eta}{\partial x_i} \\ & - \frac{g}{\rho_0} \int_{x_3}^{\eta} \frac{\partial \rho'}{\partial x_i} dx_3 + \frac{\partial}{\partial x_j} \left( \nu \frac{\partial u_i}{\partial x_j} \right) - 2\varepsilon_{ijk} \Omega_j u_k \end{aligned} \quad (4.3)$$

Equation (4.3) shows how the horizontal velocity components are calculated, where  $u_i$  are the velocity vector components in the horizontal Cartesian  $x_i$  directions ( $i = 1; 2$ ),  $u_j$  are the velocity vector components in the three Cartesian directions  $x_j$  ( $j = 1; 2; 3$ ),  $p_{atm}$  is the atmospheric pressure, and  $\nu$  is the turbulent viscosity.  $\rho$  is the specific mass,  $\rho'$  is its anomaly,  $\rho_0$  is the reference specific mass,  $\eta$  is the free surface level,  $\rho(\eta)$  represents the specific mass at the free surface,  $g$  is the acceleration of gravity,  $t$  is the time,  $\Omega$  is the Earth's velocity of rotation, and  $\varepsilon$  is the alternate tensor.

The mass balance equation (continuity) is:

$$\frac{\partial u_1}{\partial x_1} + \frac{\partial u_2}{\partial x_2} + \frac{\partial u_3}{\partial x_3} = 0 \quad (4.4)$$

The density  $\rho$  is calculated as a function of temperature and salinity by the equation of state [Leendertse and Liu, 1978]:

$$\rho = ((5890 + 38T - 0.375T^2 + 3S)) / (((1779.5 + 11.25T - .00745T^2) - (3.8 + 0.01T)S^2 + 0.698(5890 + 38T - 0.375T^2 + 3S))) \quad (4.5)$$

The vertical velocity is calculated from continuity equation (4.4) by integrating between the bottom and the depth  $z$  where  $u_3$  is to be calculated:

$$u_3(x_3) = \frac{\partial}{\partial x_1} \int_{-h}^{x_3} u_1 dx_3 - \frac{\partial}{\partial x_2} \int_{-h}^{x_3} u_2 dx_3 \quad (4.6)$$

To obtain the free surface equation, the Continuity Equation (4.2) is integrated over the whole water column. The integration limits are the free surface elevation,  $\eta(x, y)$ , and the bottom,  $-h$  (where  $h$  is the depth).

$$\frac{\partial \eta}{\partial t} = -\frac{\partial}{\partial x_1} \int_{-h}^{\eta} u_1 dx_3 - \frac{\partial}{\partial x_2} \int_{-h}^{\eta} u_2 dx_3 \quad (4.7)$$

The model solves a transport equation for salinity and water temperature, in this case, or any tracer for other works and studies. The formulation of the advection-diffusion equation is:

$$\frac{\partial \alpha}{\partial t} + u_j \frac{\partial \alpha}{\partial x_j} = \frac{\partial \alpha}{\partial x_j} \left( K \frac{\partial \alpha}{\partial x_i} \right) + \text{FP} \quad (4.8)$$

where  $\alpha$  is the transported property,  $K$  is the diffusion coefficient and FP is a possible source or sink term.

## 4.2 Discretization

Mohid uses a finite volume approach to perform the spatial discretization that is fully described in Martins *et al.* [2001] and Leitão [2003]. In the horizontal direction is adopted an Arakawa C staggered grid [Arakawa and Lamb, 1977].

The temporal discretization is carried out using a semi-implicit algorithm: the ADI (Alternate Direction Implicit), described in Abbott and Basco [1994]. In all simulations was used the 6 equation algorithm discretization scheme by Leendertse [1967]. This algorithm calculates alternatively one component of horizontal velocity implicitly while the other is calculated explicitly, avoiding the calculation of the internal and external modes with different time steps [Leitão, 2003].

## 4.3 Boundary Conditions

Five different types of boundaries were used in this work: bottom, free surface, lateral closed boundary, lateral opened boundary and moving boundary. At the free surface boundary all advective fluxes across the surface are assumed null which means  $W$  (vertical flux) is null:

$$Wflux|_{surface} = 0 \quad (4.9)$$

Diffusive flux of momentum is imposed assuming clearly a wind surface stress,  $\vec{\tau}_W$ :

$$v_3 \frac{\partial u_i}{\partial x_3} \Big|_{surface} = \vec{\tau}_W, i = 1, 2 \quad (4.10)$$

where  $v_3$  is the vertical eddy viscosity. The wind stress is computed according to a quadratic friction law:

$$\vec{\tau}_W = C_D \rho_a |\vec{V}| V \quad (4.11)$$

where  $\vec{V}$  is the wind speed measured 10 m above the sea surface,  $\rho_a$  is the air density and  $C_D$  is a drag coefficient which is a function of the wind speed. In this work, the wind stress forcing was not considered.

The bottom shear stress is calculated using a non-slip method with a quadratic law which depends on the near bottom velocity:

$$v_3 \frac{\partial u_i}{\partial x_3} \Big|_{bottom} = C_D u_i \sqrt{u_1^2 + u_2^2}, i = 1, 2 \quad (4.12)$$

In the 2D mode, the bottom drag coefficient ( $C_D$ ) is calculated based on the Manning coefficient ( $n$ ):

$$C_D = gn^2 H^{1/3} \quad (4.13)$$

While for the 3D mode the  $C_D$  calculation is based on a logarithmic law and on the von Karman constant ( $k$ ) (4.14):

$$C_D = \frac{k}{lg \frac{z_l + z_0^b}{z_0^b}} \quad (4.14)$$

where  $H$  ( $H = h + \eta$ ) is the depth of the water column,  $z_0^b$  is the bottom roughness length and  $z_l$  is the distance from the bottom to the middle point at each layer.

At the ocean open boundary the free surface elevation is imposed and at the river boundaries the flow is specified. A free slip condition is imposed at the lateral boundary condition by specifying a zero normal component of mass and momentum diffusive fluxes at cell faces in contact with land.

Moving boundaries are closed boundaries whose position varies with time. In domains with large intertidal zones, like Ria de Aveiro, are very frequent. The uncovered cells must be tracked and with this purpose a criterion base in Figure 4.1 is used.  $H_{MIN}$  is the depth bellow which cell is considered uncovered. In this case a thin volume of water above the uncovered cell is conserved. The cell of position  $i, j$  is considered uncovered when one of the two following situation is true [Leitão, 2003; Vaz, *et al.*, 2005]:

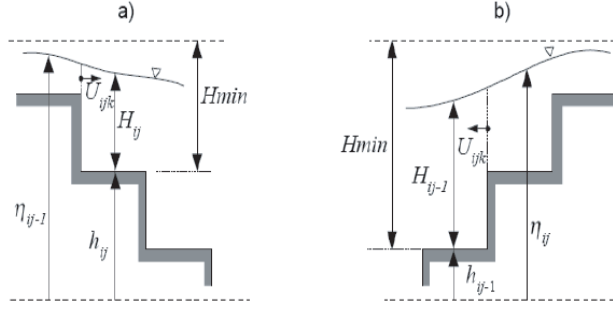


**Figure 4.1: Conditions for a cell to be considered uncovered (moving boundaries) [Leitão, 2003].**

$$H_{ij} < HMIN \wedge \eta_{ij-1} < -h_{ij} + HMIN \quad (4.15)$$

$$H_{ij-1} < HMIN \wedge \eta_{ij} < -h_{ij-1} + HMIN \quad (4.16)$$

The second condition of (4.15) assures that the cell is not being covered by the tidal wave propagating from left to right and the second condition of (4.16) assures that the cell is not being covered by the tidal wave propagating from right to left. The noise formed by the abrupt change in velocity at the dry cells is controlled with a careful choice of  $HMIN$  (in this simulation:  $HMIN = 0.10$  m) [Leendertse and Liu, 1978].

#### 4.4 Surface heat fluxes parameterizations

The interaction between air and water in shallow water systems, like the Ria de Aveiro, is of extreme importance and it also influences the temporal variability of the various physical, chemical and biological processes. The water-air heat exchanges are determined by five distinct processes: atmospheric longwave radiation, solar shortwave radiation, water longwave radiation, and sensible and latent heat flux. In Mohid, the total heat surface flux is obtained summing the three last processes referred before. The solar and atmospheric radiation entering in the water column is parameterized as exponential function of depth by the law proposed by Kraus [1972]:

$$I(z) = F_{sol} \left( I_1 e^{-z/\lambda_1} + I_2 e^{-z/\lambda_2} \right), I_2 = 1 - I_1 \quad (4.17)$$

$I_1$  and  $I_2$  refer to the long and shortwave radiation component, respectively.  $z$  is positive downward, being  $z = 0$  the sea surface. The values of  $I_1$ ,  $\lambda_1$ , and  $\lambda_2$  where published by Paulson and Simpson [1977] according to the classification found in Jerlov [1968].

Mohid uses the formulation found in Brock [1981] to quantify the incoming solar radiation in the water surface which depends on the sun height, atmospheric absorption and albedo:

$$R_s = (1 - albedo) \times QS_0 \times AT \times neb \quad (4.18)$$

$R_s$  is the incoming solar radiation [ $\text{Wm}^{-2}$ ],  $QS_0$  is the Solar Constant [ $\text{Wm}^{-2}$ ],  $AT$  is the atmospheric transference,  $neb$  is the nebulosity (% of cloud cover). The net longwave radiation  $R_a$  [ $\text{Wm}^{-2}$ ] is calculated using [Swinbank, 1963]:

$$R_a = 0.937 \times 10^{-5} \sigma (273.15 + T_a)^6 (1 + 0.17 neb^2)(1 - R_e) \quad (4.19)$$

where  $\sigma$  is the Stefan-Boltzmann constant ( $5.6697 \times 10^{-8} \text{ Wm}^{-2}\text{K}^{-4}$ ) and  $R_e$  is the radiation reflected by the sea surface (%).  $R_{br}$  [ $\text{Wm}^{-2}$ ] (infrared radiation) is calculated applying the Stefan-Boltzmann law:

$$R_{br} = \varepsilon \times \sigma \times (273.15 + T_w)^4 \quad (4.20)$$

where  $\varepsilon$  is the water emissivity ( $\sim 0.97$ ) and  $T_w$  is the water temperature [K]. The latent  $H_L$  and sensible  $H_S$  heat fluxes [ $\text{Wm}^{-2}$ ] are obtained using the Dalton and Bowen laws, respectively (adopted from Chapra [1997]):

$$H_L = (19.0 + 0.95U_w^2) \times (e_{s,w} - r_h \times e_{s,a}) \quad (4.21)$$

$$H_S = C_b \times (19.0 + 0.95U_w^2) \times (T_w - T_a) \quad (4.22)$$

The  $U_w$  is the wind speed [ $\text{ms}^{-1}$ ],  $e_{s,w}$  is the saturated water pressure [mmHg],  $r_h$  is the relative humidity [values ranges from 0 to 1],  $e_{s,a}$  is the air saturation pressure [mmHg],  $C_b$  is the Bowen coefficient [ $\sim 0.47 \text{ mmHGK}^{-1}$ ],  $T_w$  and  $T_a$  is the water and air temperature [K]. The latent heat flux is directly related to pressure vapour deficit and sensible heat is related to the water-air temperature difference.



## 5 Hydrodynamic Model Implementation to the Ria de Aveiro

### 5.1 Numerical Grid Construction

Apart of the boundary conditions, the bathymetry is probably the most important factor that affects the flow in shallow waters systems such as Ria de Aveiro. The bathymetry controls the spatial variability of the current magnitude and direction, constituting a factor which ensures the realism of the numerical model [Cheng *et al.*, 1991; Dias and Lopes, 2006].

Over the last years, the Ria de Aveiro hydrodynamics has been extensively studied using numerical modeling tools (Dias *et al.*, 1999, 2000; Vaz *et al.* 2005, 2007; Picado *et al.*, 2010). However, the large areas of low lying lands that surround this lagoon were not described in the numerical grids used for the previous hydrodynamic modeling applications. Although the study of the mean sea level rise effects in Ria de Aveiro hydrodynamics is not an aim of this work, this low lying lands will probably be frequently flooded in the near future [IPCC, 2007], why justifies the inclusion of these data in the numerical bathymetry to develop this work

In order to build a numerical grid for Ria de Aveiro, a preliminary actualization of available bathymetric data for the lagoon was performed with the most recent sounding information using the ArcGis® software. The main data base concerning depth sounding values for Ria de Aveiro was obtained from a general survey carried out in 1987/88 by the Hydrographic Institute of Portuguese Navy (IH). This depth database was updated using field data from several recent surveys performed by the Harbor Administration (APA) at the inlet channels and by the Hydrographic Regional Administration (ARH) at S.Jacinto channel. It was also updated with topography data from an available Digital Terrain Model for the adjacent low lying lands (Figure 5.1).

Two numerical bathymetries were developed in order to evaluate the importance of including the low lying lands when simulating the lagoon hydrodynamics. The first one comprises data until 2 meters above the local datum (grid 1), and the other until 7 m above the local datum (grid 2), with the adjacent low lying lands. In order to eliminate grid irregularities which may constitute a cause of instability, and to ensure that there are no closed channels and that all the water may circulate, the previous numerical grids were manually corrected using MohidGIS software based in Google Earth® software observations. Finally, the numerical rectangular grid developed had 387 by 219 cells in  $y$  and  $x$  directions, respectively, with a spatial resolution of 100 m (Figure 5.1).

Mendes *et al.* [submitted] adopted a methodology to compare hydrodynamic changes induced by the use of these two numerical grids. After the Mohid-2D model implementation for the Ria de Aveiro and in order to evaluate tidal changes induced by considering the adjacent low lying lands, it were computed the velocity fields for the two grids used in this simulation. It was also performed harmonic analysis (Pawlowicz *et al.*, 2002) to sea level height and current velocity model outputs for both grids. Moreover, ellipse parameters were assessing to complement the comparison of the numerical bathymetries. Mendes *et al.* (submitted) follow the Xu (2000) methodology which defined four parameters to the ellipses: the Semi-Major Axis of ellipses (SEMA) corresponds to the maximum current velocity value at each station; the angle between SEMA and the northern semi-major axis is the preferential flow direction (inclination (INC)); and

the eccentricity (ECC) is the ration of semi-minor to semi-major ellipses axis and evaluates the direction time variability.

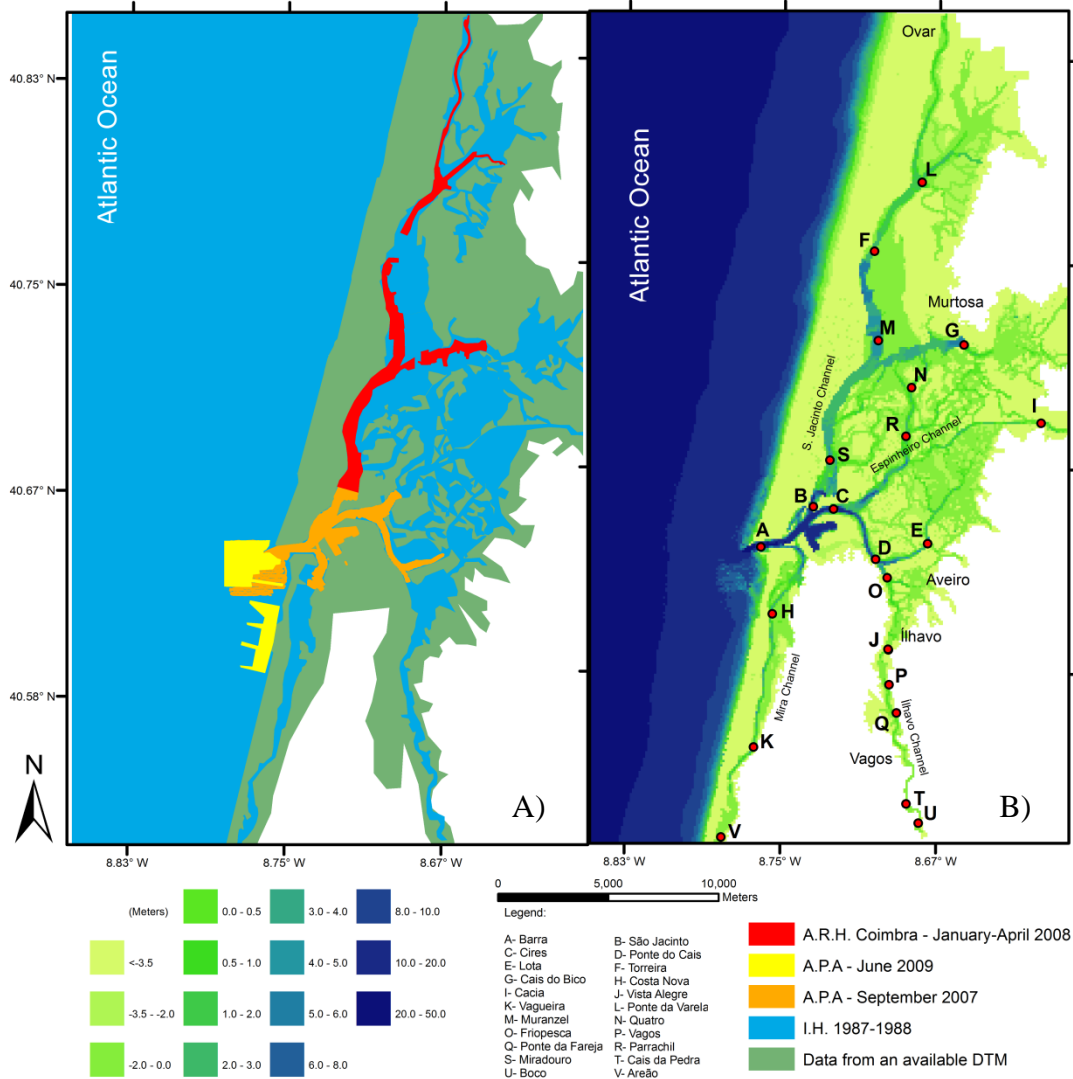


**Figure 5.1: A) Map of depth databases used in numerical bathymetry actualization. B) Numerical grid of the Ria de Aveiro lagoon.**

The results show that the maximum speed during the simulation period reached  $2.62 \text{ ms}^{-1}$  for the numerical grid 1, while for the numerical grid 2 the maximum was  $2.71 \text{ ms}^{-1}$ . Near the mouth of the lagoon the mean velocity modulus variation is  $\sim 0.02 \text{ ms}^{-1}$ . This deviation increases in the central areas and in the northern S. Jacinto channel. The maximum difference in those areas is  $0.10 \text{ ms}^{-1}$ . Close to the low lying lands the velocity is typically lower than  $1 \text{ ms}^{-1}$ .

The SEMA difference values are significantly higher ( $0.02 \text{ ms}^{-1}$  for the  $M_2$  and  $0.01 \text{ ms}^{-1}$  for the  $S_2$  constituent close to the mouth of the lagoon). These results are consistent with the velocity values. There is also a phase delay between both simulations. For the  $M_2$  and the  $S_2$  constituents, this delay is higher at northern S. Jacinto channel ( $\sim 5$  minutes). The ECC in all stations is near zero which represents a current polarization in one direction.

Figure 5.2A) reveals that the relative differences between the  $M_2$  amplitude (for both grids) are almost negligible ( $< 5\%$ ). Moreover, the phase difference (Figure 5.2B)), over the entire length of the lagoon never exceeds  $5^\circ$  ( $\sim 10$  minutes). For the  $S_2$ , the relative differences in amplitude are slightly larger when compared with the  $M_2$  constituent but never exceeding  $7\%$  of local constituent amplitude range (Figure 5.2C). The  $S_2$  phase differences reach values of around  $10^\circ$  (20 minutes) (Figure 5.2D). The major deviations values, either in amplitude and phase of the two harmonic constituents, are located in the areas with a large concentration of narrow channels which include an adjacent low-lying land area. It is clear that the differences are amplified from the lagoon mouth to the upstream areas.

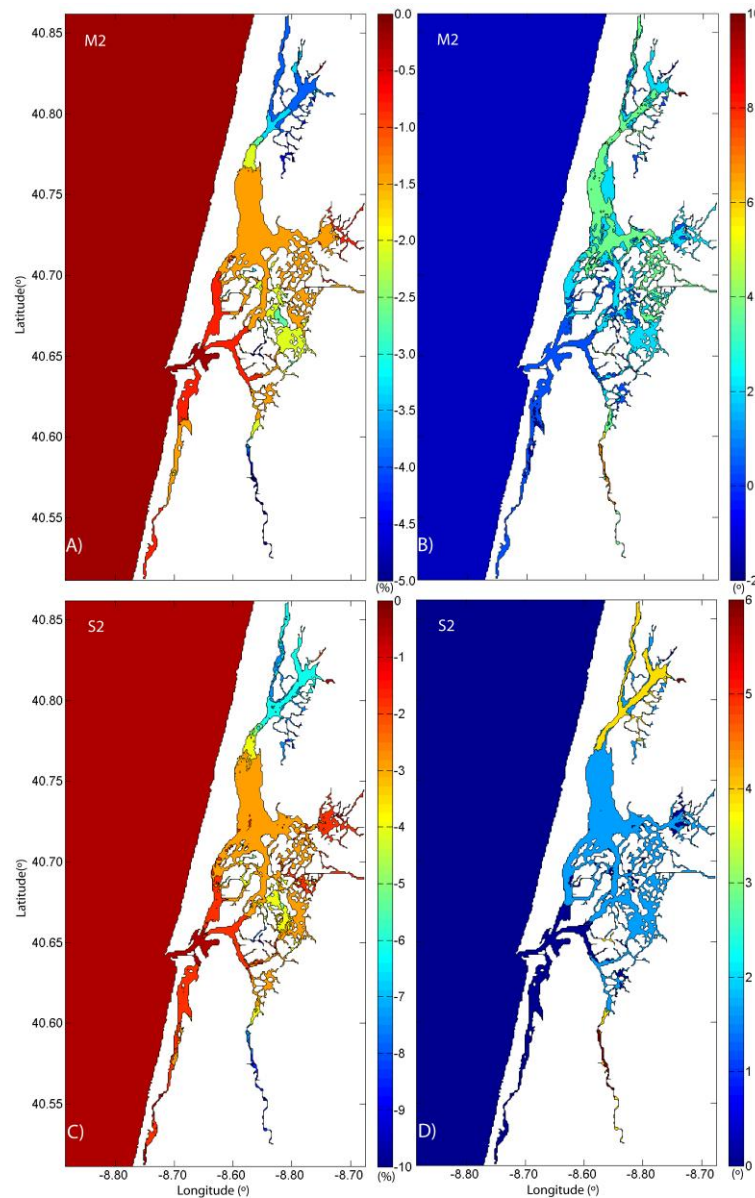


**Figure 5.2:** A) Relative difference of  $M_2$  amplitude between grid 1 (data from 2 m above local datum) and grid 2 (data from 7 m above local datum). B) Phase difference of  $M_2$  between grid 1 and grid 2; C) Relative difference of  $S_2$  amplitude between grid 1 and grid 2; D) Phase difference of  $S_2$  between grid 1 and grid 2.

The Mendes *et al.* [submitted] study reveals that although the differences in the numerical results for the general circulation of the Ria de Aveiro are negligible when considering the low lying coastal adjacent flooded areas, some consistent patterns were found that suggest that the inclusion of these areas are important for more accurate studies. The velocity differences patterns and SEMA results are consistent with the results reported by Picado *et al.* [2010], where show how a 5.6% increase in the Ria de Aveiro flooded area due to the deterioration of the local salt pans walls corresponding to an increase of about 5-6% of the tidal currents intensity. Thus, the grid 2 is implemented in this work to ensure that future studies on extreme events in Ria de Aveiro lagoon (extreme river discharges, mean sea-level rise, *storm surges*, etc) can be done with this model configuration.

## 5.2 Hydrodynamic Model Calibration

The model calibration is based on the adjustment of parameters to which the model is most sensitive. In Ria de Aveiro, according to Dias and Fernandes [2006], the magnitude of the bottom friction coefficient determines changes in the tidal wave propagation within the lagoon. Thus, in order perform the model calibration the tuning parameter is the Manning coefficient ( $n$ ) (Equation 4.13). A Manning coefficient grid was constructed, based on values used by Vaz *et al.*, [2007], and localized fine-tuning had been done based on the Hsu *et al.* [1999] procedure.

In this work, the model calibration was carried out by comparing observed surface elevation data with model results, and by comparing the amplitude and phase of the harmonic tidal constituents. For the model calibration, the data available are from field works carried out in Ria de Aveiro 2003. All data were collected in the framework of the PhD Thesis of Araújo [2005] and the measurements were performed every six minutes, except in station F where measurements were done every half hour. At the open ocean boundaries, the free surface elevation was specified from 50 tidal constituents obtained after harmonic analysis [Pawlowicz *et al.*, 2002] of data measured at a tide gauge located close to the lagoon mouth, during 1987. These tidal constituents were imposed at the ocean open boundaries with a phase and amplitude corrector factor in a way that the model results reproduce the free surface elevation at station A (lagoon mouth).

### 5.2.1 Results

The calibration was performed at 11 stations within lagoon. Figure 5.3 shows the comparison between the computed and observed SSE time series for two days in each station. The model performance was measured by RMS errors and using a Skill parameter:

$$RMS = \left\{ \frac{1}{N} \sum_{i=1}^N [\zeta_0(t_i) - \zeta_m(t_i)]^2 \right\}^{1/2} \quad (4.23)$$

$$Skill = 1 - \frac{\sum |\zeta_m - \zeta_0|^2}{\sum [|\zeta_m - \bar{\zeta}_0| - |\zeta_0 - \bar{\zeta}_0|]^2} \quad (4.24)$$

Where  $\zeta_0(t)$  and  $\zeta_m(t)$  are the observed and computed SSE, respectively,  $N$  is the number of measurements in the time series,  $\zeta$  is sea surface elevation and  $\bar{\zeta}$  the time mean. Based in Dias *et al.* [2009] the RMS values should be compared with the local tidal amplitude and if those errors are lower than 5% of the amplitude, the agreement between model and observations results should be considered excellent and if they range between 5% and 10% the agreement should be considered very good. In the case of predictive model Skill, a method was developed by Wilmott [1981] and recently used by Warner *et al.* [2005] and Li *et al.* [2005], the perfect agreement between model results and observations yield a Skill of one and complete disagreement yield a skill of zero. Skill values higher than 0.95 should be considered representative of an excellent agreement between model results and observations [Dias *et al.*, 2009].

It is important to note that in order to compare model results with measurements the low frequency signal was removed from the data, considering a cut-off frequency of 0.0000093 Hz (30 h). In general, the results revealing an accurate reproduction of SSE in the Ria de Aveiro lagoon. The RMS values ranges from 2.2% to 9.8% of the local amplitude in all stations. Thus, the agreement between predictions and observations, in all stations, ranges from very well to excellent.

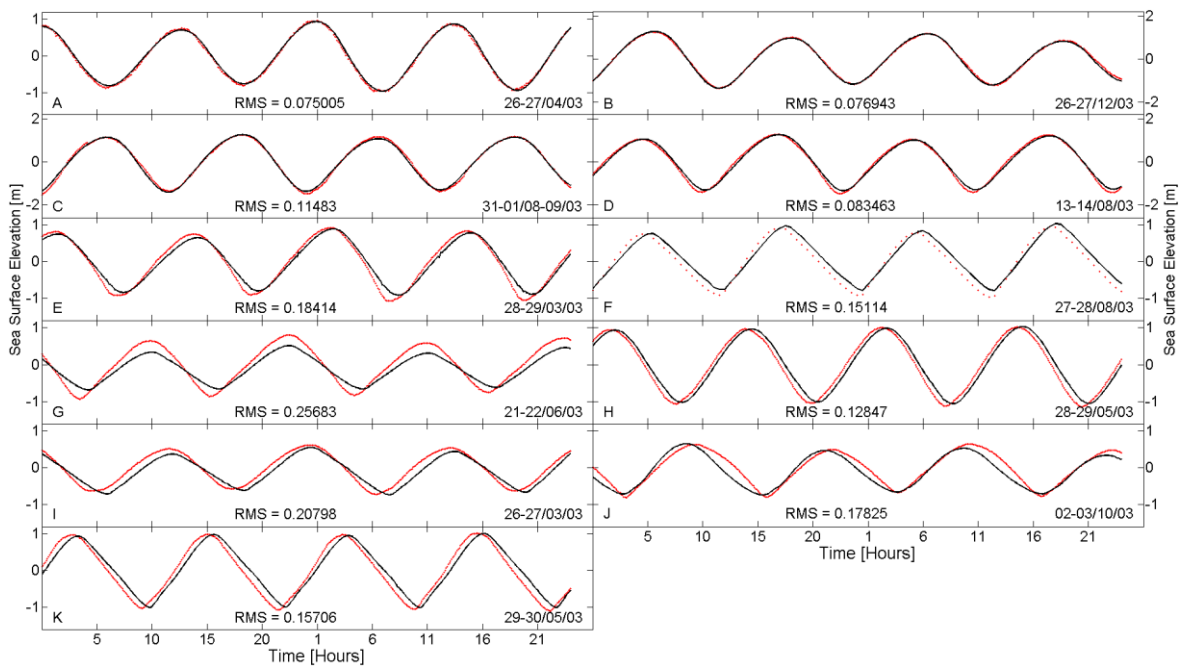


**Figure 5.3: Comparison between SSE time series for stations A, B, C, D, E, F, G, H, I, J, and K used in the hydrodynamic calibration procedure (● red: data; black solid line: model).**

At station A, the computed and observed data comparison should be perfect. The difference is ~7 cm, which represents an error of 2.2% when it was compared with local tidal amplitude. This difference may be justified by an ineffective tidal phase and amplitude correction factor from the open boundary to station A, or considering that the same phase and amplitude values for all the tidal constituents were imposed in all the open ocean boundaries (north, west, and south boundaries), not taking into account with the local differences. This small error may partially explain the errors found in the other stations within the lagoon. In stations A, B, C, D and H the disagreement is lower than 5% of local tidal range. In general, the errors increase with the distance

between the station and the lagoon mouth. This justification can be set for all stations, except for the station G, where the error is higher ( $RMS = 0.26$  m). This difference can be explained for the gap of actual bathymetric data in the area before the station (Figure 5.1). Other important error source is the inaccurate definitions of bathymetry. For example, the Ílhavo channel has, in some sections, a width of 10 m, causing a complete misfit when it is considered a numerical grid cell with 100 m. The Skill values in all stations are higher than 0.95, except in station G, representing an excellent agreement between model forecasts and observations.

The direct comparison of RMS errors and Skill parameter has the disadvantage of quantifying phase lags over time series. Consequently, in this work it was also performed a harmonic analysis [Pawlowicz *et al.*, 2002] of the predicted and observed SSE in order to quantify separately the amplitude and phase lags for all stations (Figure 5.4).

The tidal constituent comparison shows major disagreement at the upstream stations. Furthermore, station G results reveal an important discrepancy, mainly in the  $M_2$  and  $M_4$  amplitude and phase when compared with other stations.

It is important to focus that the most significant differences are for constituents  $M_2$  and  $S_2$ , which represent  $\sim 90\%$  of the tidal energy in Ria de Aveiro lagoon [Dias *et al.*, 1999]. The analysis of these results shows that the mean amplitude difference, in all stations, for the  $M_2$  component is about 8 cm, and the mean phase difference is about  $8^\circ$ . This value corresponds to a difference of about 16 minutes in the arrival of tidal wave. But, in the station near the lagoon mouth (Station A) this difference is much smaller than the average value (less than 30 s in phase and 1.5 cm in amplitude). For the  $S_2$  constituent, the mean amplitude and phase deviation in all stations is higher. The mean amplitude difference is  $\sim 3$  cm and phase difference is  $10^\circ$ , which means that the average delay is about 20 minutes.

For the  $N_2$  constituent and the diurnal constituents  $K_1$  and  $O_1$  the deviation pattern in amplitude and phase is very similar with the other components referred before ( $M_2$  e  $S_2$ ). It is important to explain that the apparent error present in the  $O_1$  phase at stations J e K only appears in Figure 5.4: Figure 5.4 because of the adopted graph scale. Actually, the difference between the predicted and observed  $O_1$  phase is  $\sim 16^\circ$  (69 minutes) at station J and  $\sim 23^\circ$  (98 minutes) at station K. The mean  $N_2$ ,  $K_1$  and  $O_1$  amplitude difference in all stations, compared with the mean constituent amplitude is 10%, 18% and 11%, respectively. Regarding the phase of these constituents, the mean difference is about  $9^\circ$  (19 minutes),  $13^\circ$  (52 minutes), and  $11^\circ$  (78 minutes), respectively.

The  $M_4$  is a harmonic constituent which represents a short-period harmonic term in order to take into account the change in the form of a tidal wave resulting from shallow water condition. In shallow waters the progression of a tidal wave is modified by several physical factors which depend on the square or higher powers of the tidal amplitudes. The relationship involving the square of the amplitude has produced additional harmonics ( $M_4$  example for the  $M_2$  tidal constituent). The relationships are more complicated because there are several types of non-linear activity which influence the dynamics: bottom friction, effects due to the water depth being comparable to the tidal amplitude, and curvature imposed on the flow patterns by topography [Pugh, 1996]. In summary, the generation and/or enhancement of  $M_4$  component are related with the water depth and channels/estuary geometry.

The model forecasts show that the  $M_4$  harmonic constituent reproduction is not as accurate as for the other constituents. This mismatch can be explained by some bathymetric errors and by the fact of that numerical grid resolution used implies some inaccuracies in reproducing the

complex geometry of the Ria de Aveiro lagoon. The  $M_4$  mean difference for all stations is about 2.3 cm (40% of the mean amplitude) and the phase delay is about  $11^\circ$ , which represent 11 minutes. Nevertheless, the results for the  $M_4$  constituent are considered accurate for the purposes of this work.

Although the differences between model predictions and field data it is concluded that the hydrodynamic calibration was successfully reached.

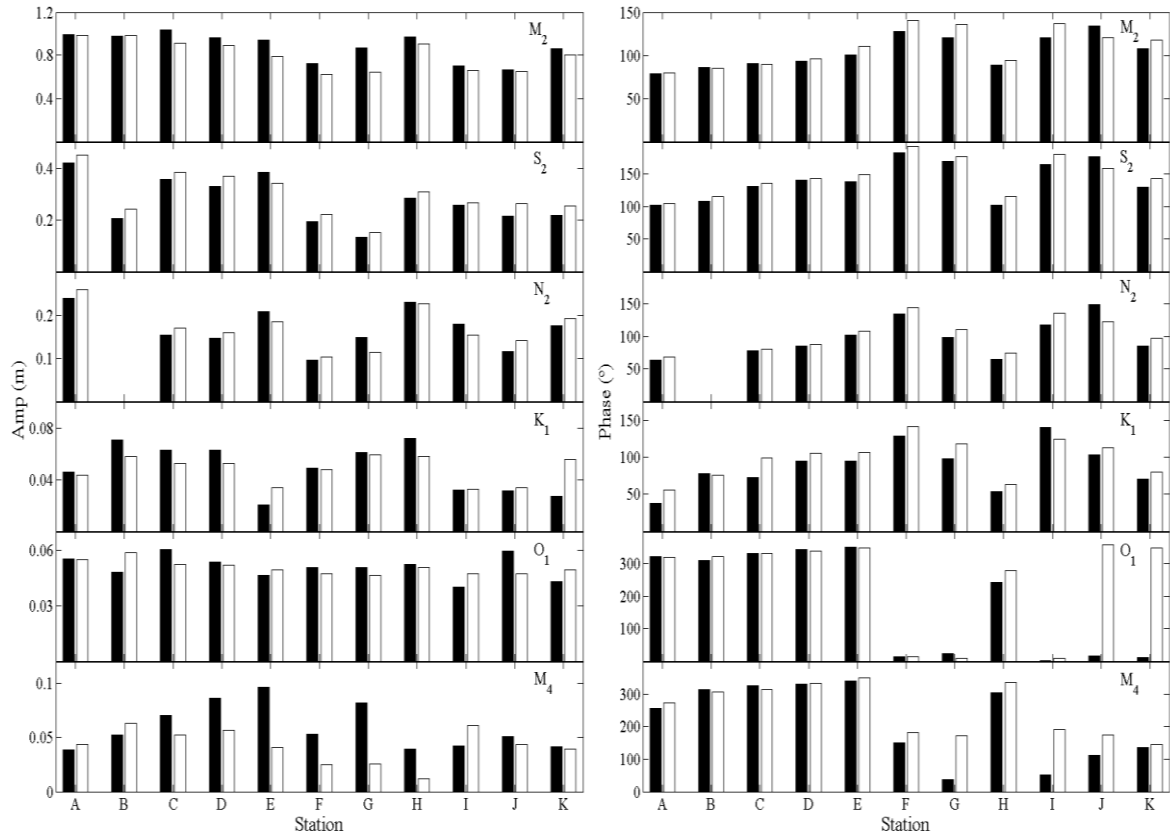


**Figure 5.4:** Comparison between model predicted and observed amplitude and phase for the major semi-diurnal and diurnal constituents ( $M_2 - 12.42$  h;  $S_2 - 12$  h;  $N_2 - 12.9$  h;  $K_1 - 23.93$  h;  $O_1 - 25.82$  h) and for the shallow water overtide of the principal lunar constituent,  $M_4$  (6.21 h). The black and white bars represent the observed and predicted values, respectively.

### 5.3 Hydrodynamic Model Validation

The validation of a model is a procedure for testing the models predictions accuracy with an independent observed data set. The data used to perform this task correspond to a period during June 1997, where model performance was evaluate by comparing RMS errors between time series of predicted and observed SSE, and of current velocity for eleven and ten stations, respectively.

#### 5.3.1 Results

The procedure was carried out without any change in the tidal input characteristics and in the correction factor, referred in the calibration procedure. Also, the Manning coefficients were not modified.

It is important to note that regarding the comparison of current velocity, the values change rapidly in space, both in magnitude and direction, from point to point. This behavior of the velocity magnitude and direction reflects the irregular geometry of the lagoon. The bathymetry influence and the fact that the model results represent the average over the vertical (and horizontal), and that field data are measured in a single point value is significant to justify some expected differences. In order to compare the velocities, the main flow direction was found for measurements and predictions at each station. These directions were almost coincident and the current velocities values were projected along them. The perpendicular flow direction velocities are almost null and were not considered. The results are shown in Figure 5.5 and Figure 5.6.

The RMS errors for the SSE range from 3 to 8% at six stations (B, H, J, O, P, and Q) and between 12 e 16% at the other four stations. Figure 5.5 shows a pattern similar to that obtained for the calibration procedure. The discrepancies are larger in the Mira and North of the São Jacinto channels. These differences can be explained with the use of older bathymetric values for the Mira channel and with the gap of bathymetric values in the area near station F. In the other stations the agreement between observed and computed results is rather good.

In the case of the current velocity comparison, it is verified that there are larger differences than those obtained for the SSE validation. In this case the RMS errors are very high. These errors vary between 12% and 50% for all stations, except in station Q where the error is 89%. This value is linked to the magnitude of current velocity, which is lower than in the other stations. Indeed, the lower values are more susceptible to errors due to the rapid changes of magnitude and direction. The location of this station can be the other reason for the large error found. Station Q is located at the end of Ílhavo channel, which is characterized by narrow areas that are not well resolved by the numerical grid used in the simulations (100 m). The error of the 50% in station K and of 32% in station L and P can be explain by the same reasons referred for the SSE validation procedure discussion. The results near the lagoon mouth and for the stations located at the main channels (Espinheiro, South of São Jacinto, North of Mira and Ílhavo channels) show lower RMS errors, revealing a good reproduction of the observed data set.

According to these results, it may be considered that the model reproduces with sufficient accuracy the SSE and current velocity data for these stations despite some differences between them. Therefore, it may be concluded that the hydrodynamic model is validated.

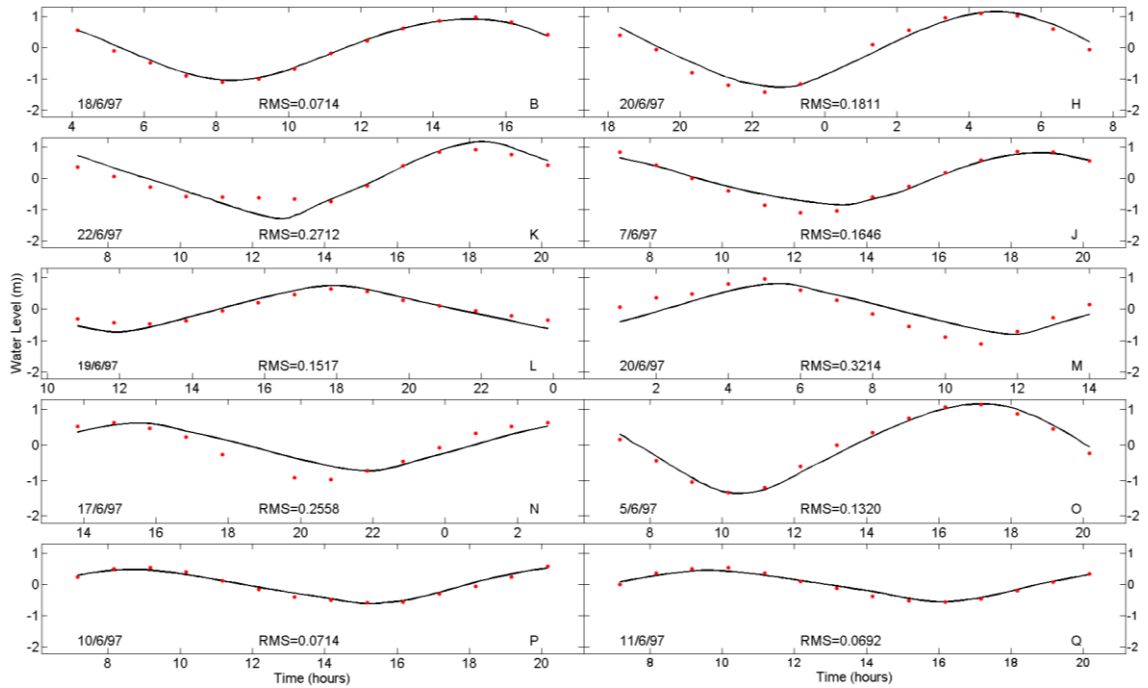


Figure 5.5: Comparison between SSE time series for stations B, H, K, J, L, M, N, O, P, and Q, used in the hydrodynamic validation procedure (● red: data; black solid line: model).

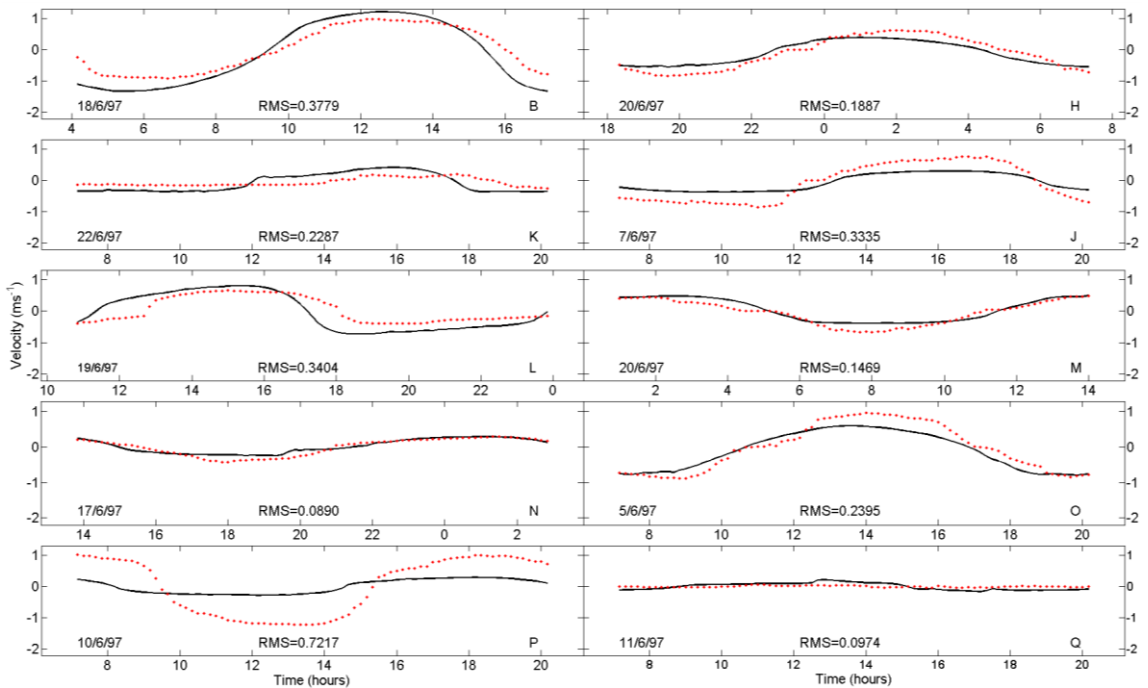


Figure 5.6: Comparison between time series of along flow direction for stations B, H, K, J, L, M, N, O, P, and Q, used in the hydrodynamic validation procedure (● red: data; black solid line: model).



## 6 Calibration and Validation of the Salt and Heat Transport Model

### 6.1 Introduction

Assuming that the barotropic flows have been calibrated and validated for the Ria de Aveiro, the procedure used to calibrate the salt and heat transport consists in comparing measured and predicted salinity and temperature time series for several stations distributed along the main lagoon channels. In the study area (shallow water system), the horizontal patterns of water temperature are strongly influenced by the exchanges between the atmosphere and the water surface. These patterns adjust dynamically to different sea and lagoon water temperature, and also to meteorological forcing. Vaz [2007] illustrates how the meteorological forcing affects the water temperature and concludes that the major changes in the temperature horizontal patterns are visible after 12 tidal cycles in the model simulations.

### 6.2 Calibration

#### 6.2.1 Data set and Methods

The measurements used for the salt and water temperature calibration were obtained during July 1996 (from 09/07/1996 to 28/07/1996). The set includes a 25 hours time series of hourly data measured at seven different stations distributed along the lagoon. These observations were performed after a long dry period, where the rivers flows input are expected to be low. The meteorological data were imposed from the NCEP data base (nearest grid point: 40.953 °N, -9.375 °W), concurrent with the simulation periods. At the ocean open boundary was specified a salinity value of 36.5 psu and a water temperature of 14 °C. The rivers flows were not known for this period and are used as a calibration parameter. The river discharges values used here were: Vouga river-  $2 \text{ m}^3\text{s}^{-1}$ ; Antuã river-  $0.5 \text{ m}^3\text{s}^{-1}$ ; Boco river-  $0.2 \text{ m}^3\text{s}^{-1}$ ; Valas de Mira-  $2 \text{ m}^3\text{s}^{-1}$ ; Caster river-  $0.5 \text{ m}^3\text{s}^{-1}$ ; and Gonde river-  $0.5 \text{ m}^3\text{s}^{-1}$ . The fluvial water temperature was also specified: Vouga river- 18 °C; Antuã river- 23 °C; Boco river and Valas do Mira- 18 °C; and Caster and Gonde rivers- 25 °C. The salinity values were specified as 0 psu for each.

It was chosen to simulate a spin-off period of 20 days (the time to dynamic equilibrium is much longer than for the hydrodynamics), starting only with tidal and freshwater input. The result of this simulation was used as the initial salinity field condition. The salinity field, in Mohid, is independent of meteorological data. In another simulation it was computed the water temperature initial field condition. It was simulated a spin-off period of 7 days. Therefore this methodology doesn't require a large computational time and by assumption becomes a more realistic way of representing the initial salinity, or water temperature, field. After the dynamically adjustment, the time step to select the water temperature field is the same as for the salinity initial condition. Both heat and salt diffusion coefficients were set to  $5 \text{ m}^2\text{s}^{-1}$ .

The simulation for the models calibration was performed using the water temperature and salinity initial fields previously calculated. The heat and salt transport computation begun at the time step correspondent to initial field instant in order to not compromise the results. Also, this simulation was carrying out with the freshwater, meteorological data and tidal inputs.

## 6.2.2 Results

The comparison between computed and measured salinity data is depicted in Figure 6.1. For a quantitative assessment of the adjustment it was determined the Root Mean Square error–RMS (Section 5.2.1 in Chapter 4) for all the stations (shown in each plot).

In general, it was achieved a good agreement between predicted and measured time series. The model reproduces the salinity data in almost all stations. The phase and amplitude results show slight differences between them. During two tidal cycles the RMS values are lower than 5% of the local mean salinity for all stations, except for stations H and J. In station H the RMS value is 2.1 (~6% of the mean salinity) while in the station J the RMS error is 2.9 (~9% of the mean salinity). Those stations have higher salinity variations over time, which indicates that they are more influenced by the freshwater inputs than the other stations. The major deviations can be related to inaccuracies of real river inflow. The freshwater inflows were considered constant, which means that in the stations under stronger fluvial influence, the model cannot reproduce accurately the salinity variations.

The comparison between the model predicted and measured water temperature (Figure 6.2) shows a good agreement. The RMS error values are about 5% for B, J, L, and R stations. The errors are larger for stations D, H, and M, ranging from 8% to 14% of the local mean water temperature. These discrepancies may be due to errors when imposing the river water temperature at the land boundaries. In the water temperature modeling several other variables can introduce errors: the cloud cover variations (in this work was imposed a constant value, representing the mean value during the simulation periods); the numeric grid resolution (the solar and atmospheric radiation is parameterized as exponential function – Sector: 4.4, Chapter: 4); and in this study the spatial variations of meteorological data input were not considered.

According to these results it may be considered that the mixing processes in the Ria de Aveiro are well reproduced by the model, and that the water temperature distributions are well described by the model.

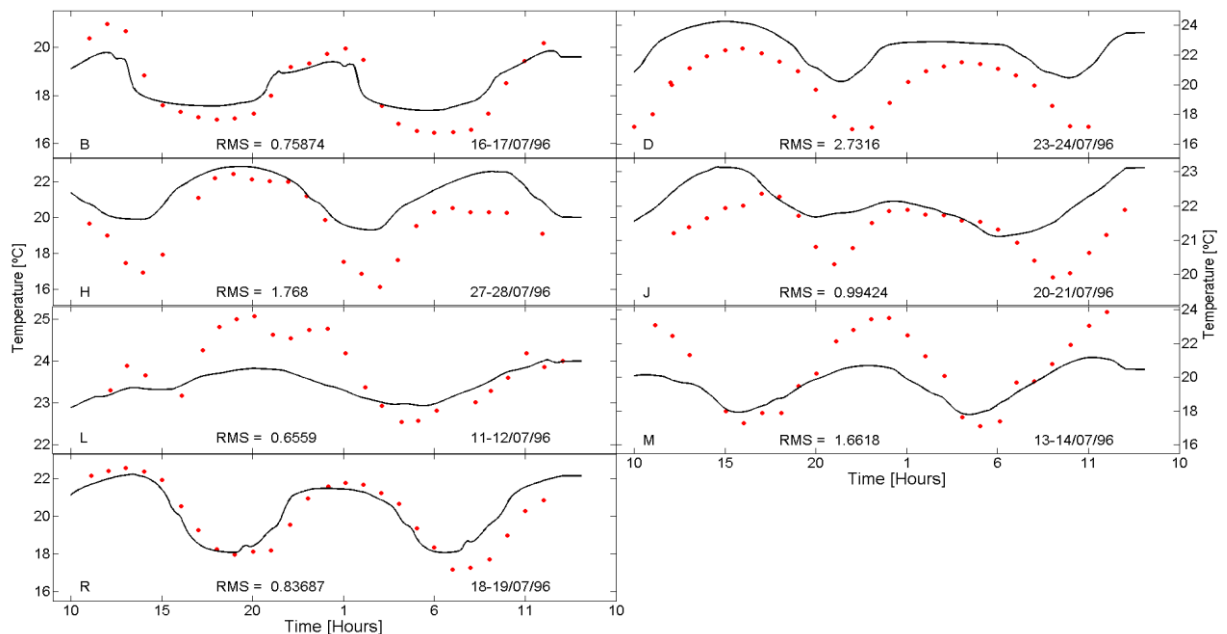


**Figure 6.1: Comparison between salinity time series for the stations used during the calibration procedure. (● red: data; black solid line: model).**

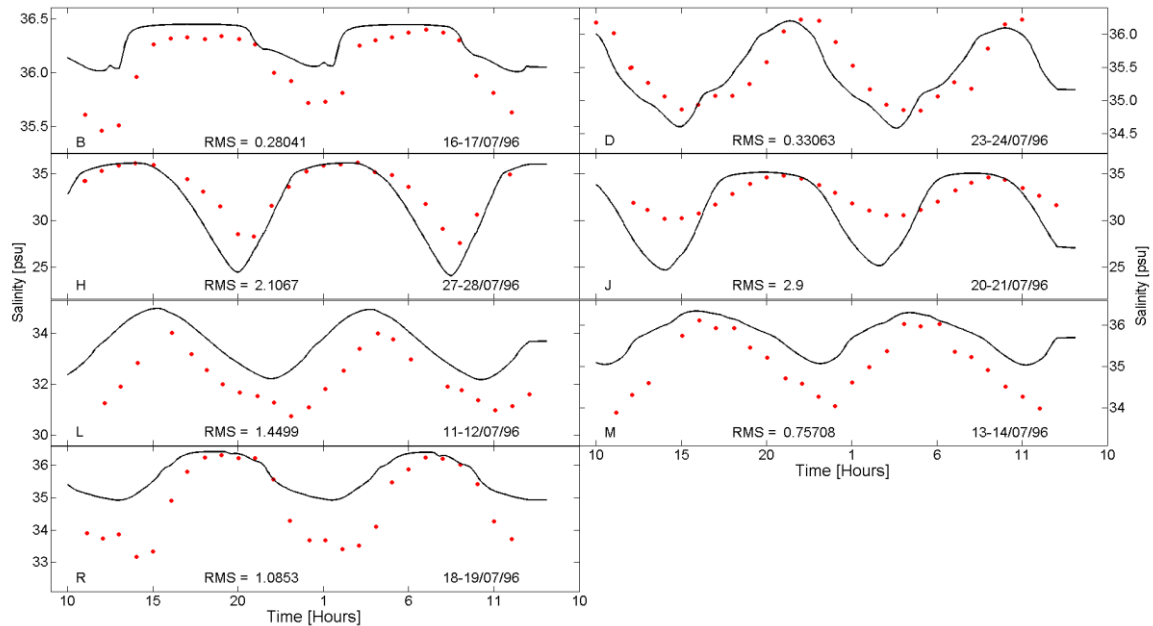


**Figure 6.2:** Comparison between water temperature time series for the stations used during the calibration procedure. (● red: data; black solid line: model).

### 6.3 Validation

The salt and heat transport model was validated through the comparison of model predictions with an independent field data set. The salinity and water temperature values are measured during June 1997 at 11 stations along the Ria de Aveiro. Here, the observed data correspond to a wet period. Consequently, the transport model is validated in different conditions than those occurred during the calibration process.

The freshwater inflows used were: Vouga river -  $13 \text{ m}^3\text{s}^{-1}$ ; Antuã river -  $11 \text{ m}^3\text{s}^{-1}$ ; Boco river -  $7 \text{ m}^3\text{s}^{-1}$ ; Valas de Mira -  $2 \text{ m}^3\text{s}^{-1}$ ; and Caster and Gonde rivers -  $3 \text{ m}^3\text{s}^{-1}$ . The freshwater temperatures were set to  $24 \text{ }^\circ\text{C}$  and the salinity was specified 0 psu. At the ocean open boundary it was specified a salinity value of 36.5 psu and a water temperature of  $18 \text{ }^\circ\text{C}$ . Once more, meteorological data from the NCEP database were used and both heat and salt diffusion coefficients were set to  $5 \text{ m}^2\text{s}^{-1}$ .

#### 6.3.1 Results

The comparison between model predictions and measured salinity and water temperature data is depicted in Figure 6.3 and Figure 6.4, respectively. It was achieved a good agreement between predicted and measured salinity values. In general the results are worst than those obtained in the calibration, as found also in the hydrodynamic calibration and validation procedures. The stations H, L, M, and S reveal a RMS error lower than 10% of the local mean salinity. Nevertheless, the amplitude in some stations is not accurately reproduced. In stations D, J, K, and R the RMS errors range from 19% to 31%. The salinity temporal evolution is well represented by the model, but the amplitude range is lower than expected. The RMS errors are higher than 50% of the local mean salinity for stations T, U, and V. These stations are located near the far end of Mira

and Ílhavo channels, near the freshwater sources, being strongly influenced by the boundary conditions that were chosen (freshwater inflow, salinity and water temperature values).

For the water temperature was found an agreement similar to that described for the calibration procedure. The RMS errors range from 1% to 22% of the local mean temperature for each station. The errors are about 5% in stations D, J, L, M, R, and S, representing a very good agreement between the predicted and measured water temperature. These results mean that the water temperature changes are very well represented by the model. The exception occurs for the stations located at the Mira channel (H: ~6%, K: ~7%, and V: ~6%). Once more, the worst results were found for the stations near freshwater sources at Ílhavo channel (T: ~8% and U: ~22%). Although the results for these stations are not very good, it is significant that they are better than those found for the salinity validation procedure. This means that the freshwater temperature values imposed on the boundary conditions are reliable. Despite the errors described, the salt and heat transport models may be considered validated. Therefore, the numerical model reproduces accurately the salinity and heat transport processes in Ria de Aveiro.

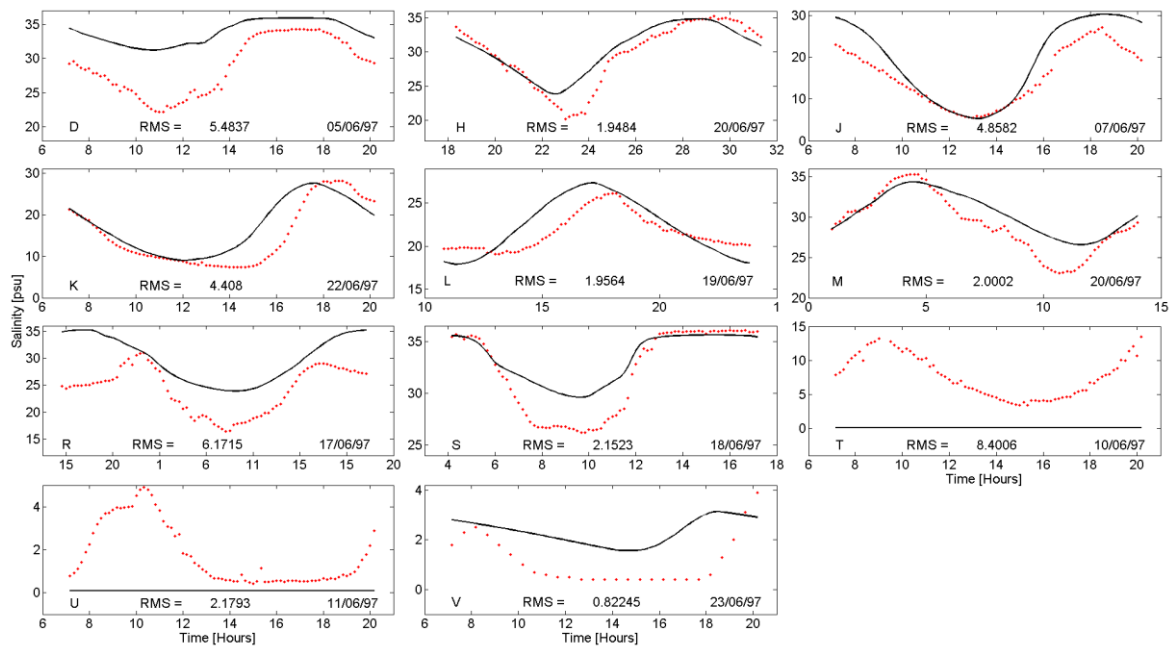


**Figure 6.3: Comparison between salinity time series for the stations used during validation procedure. (● red: data; black solid line: model).**

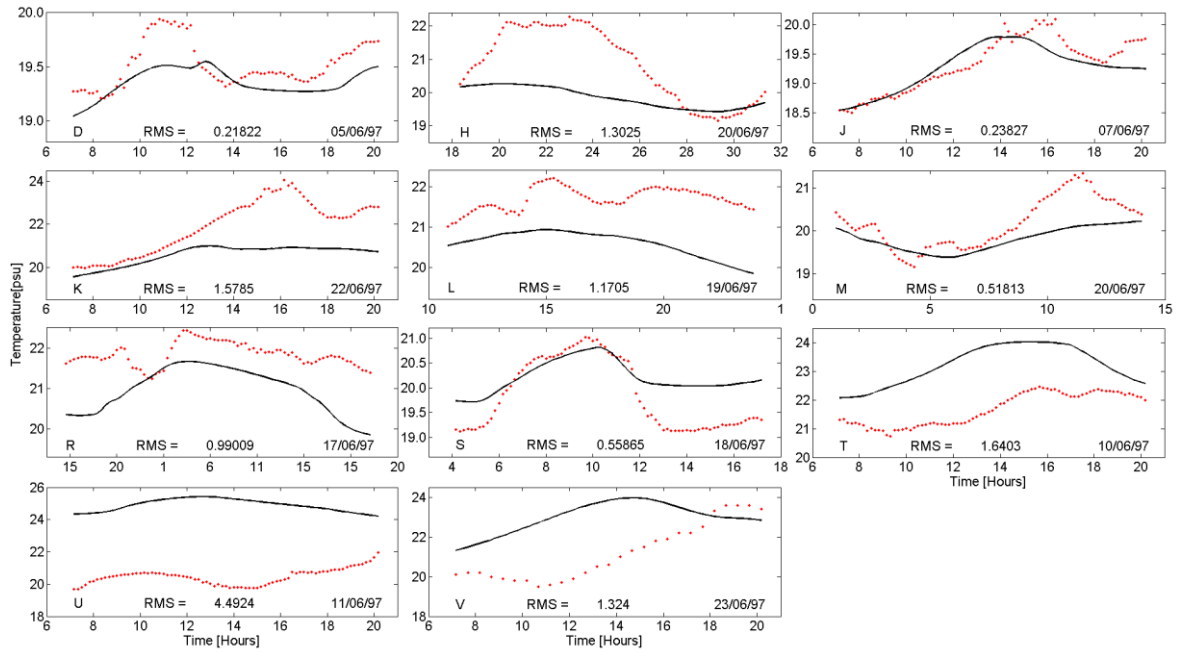


Figure 6.4: Comparison between water temperature time series for the stations used during validation procedure. (● red: data; black solid line: model).



## 7 Estuarine Plume Simulation

The nested coupled coastal models methodology was adopted in order to simulate the idealized approximation of the Ria de Aveiro estuarine plume (same pattern as in Figure 3.1).

To characterize the estuarine plume salinity stratification, with a low computational effort, it was necessary to implement a numerical model using a two level nesting configuration (Figure 7.2): the first level (D1) is a 2D barotropic tidally driven model with a variable low resolution; the second domain (D2) is a 3D baroclinic model with higher spatial accuracy where the plume propagation is expectable. In the second domain it was imposed the Ria de Aveiro discharges in one cell which corresponds to the lagoon mouth. These lagoon discharges (and its properties) are the results of the Ria de Aveiro 2D hydrodynamic model predictions (previously calibrated and validated – see Chapters 5 and 6) for three different scenarios of rivers inflows: i) typical; ii) extreme maximum; iii) and extreme minimum.

Yankovsky and Chapman [1997] formulations were calculated based on discharges values of the Ria de Aveiro 2D model simulations. Therefore, the  $y_s$  and  $h_b$  (where  $y_s$  is the distance how the plume moves offshore in an ideal model, without any exterior forcing except the inflow and  $h_b$  is the equilibrium plume depth representing a balance between buoyancy and inertial forces) were qualitatively compared with the 3D estuarine plume simulation results (see Section 3.3).

Moreover, the estuarine plume model performance was qualitatively evaluated through the comparison with the sensor TM images of the satellite LandSat7. In this procedure it was used the results of the band 6 (Thermal Infrared Band - these band values are being applied on some studies to identify surface temperature on land or water ([http://landsat.gsfc.nasa.gov/news/news-archive/soc\\_0011.html](http://landsat.gsfc.nasa.gov/news/news-archive/soc_0011.html))) in order to compare difference surface temperature patterns. The temperature data used through calibration and validation of the transport model showed that there are differences between the lagoon and the ocean water temperature. Dias [2001] and Vaz *et al.* [2005] also show that this thermal gradient in a system like the one studied in this work is strongly dependent on the balance between the spring/neap tidal cycle and the rivers inflow. According to these facts, it was chosen the day of the image based on high values of Vouga River freshwater inflow (according to [www.snirh.pt](http://www.snirh.pt)), which is the main estuarine plume forcing, and on the available images to download.

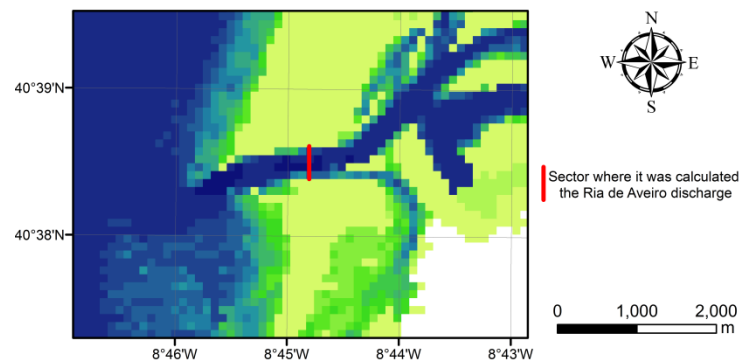
### 7.1 The Ria de Aveiro Runoff

In order to obtain the Ria de Aveiro lagoon outflow for the adjacent ocean it was decided to simulate a real period during January 2007 with the lagoon 2D model. This option had into account a future comparison and integration of the model predictions with the work carried out by Vaz *et al.*, [2009b] to study the Tagus estuarine plume. This model implementation was performed for two extreme scenarios of maximum and minimum freshwater inflow into Ria de Aveiro, corresponding to flood and dry seasons, and for one typical situation. The river discharges values were extrapolated from Génio *et al.* [2008] (Table 7.1). The salinity input is set to 0 psu in each discharge point.

**Table 7.1: River discharges values used in the Ria de Aveiro outflow simulation.**

Discharges ( $\text{m}^3 \text{s}^{-1}$ )	Vouga	Antuã	Boco	Valas de Mira	Caster	Gonde
Extreme Maximum	1000	100	5	50	5	5
Typical	150	15	5	19	5	5
Extreme Minimum	2	0.5	0.5	0.5	0.5	0.5

All simulations were carried out using the same methodology described for the 2D hydrodynamic calibration and validation model runs. In order to compute a Ria de Aveiro input for the coastal model it was compute this outflow through a longitudinal section located near the lagoon mouth (Figure 7.1).

**Figure 7.1: Location of the transversal section used to compute the Ria de Aveiro lagoon outflow.**

Hourly discharges flow through this section were determined using the magnitude values of  $v_x$  on the 4 cells that define the section (the  $v_y$  values were negligible) and the depth values for each cell. Salt and water temperature at the traversal section were determined by the mean value for these 4 cells.

## 7.2 Nested Coastal Model

As it was referred at the beginning of the Chapter 7, a two level nesting model was implemented in the coastal adjacent area of the Ria de Aveiro lagoon (Figure 7.2). The two numerical grids were created based on bathymetric values from Etopo database (<http://www.ngdc.noaa.gov/>). D1 is a 2D barotropic tidally driven model, which uses the FES2004 global solution [Lyard *et al.*, 2006] as forcing, and has variable horizontal resolution ( $0.02^\circ$ -  $0.04^\circ$ ). This model domain covers most of the Atlantic coast of the Iberia and Morocco. D2 level is a 3D baroclinic model which has  $0.01^\circ$  of horizontal resolution; including an area from the north of Mondego estuary to the Minho estuary, extending  $\sim 50$  km offshore. The domain D2 has a  $142 \times 43$  cells in  $x$  and  $y$  directions, respectively.

A sigma-level vertical discretization was adopted for the 3D model, with D2 having 20 vertical layers in average and extreme minimum outflows simulations and 15 layers in case of extreme maximum outflow. This difference is linked to some computational problems related to vertical viscosity and/or to the time step chosen during the simulations tests. On the bottom, the shear friction stress is imposed based on Equation 4.14 and the vertical viscosity and diffusivity are computed by the non-dimensional General Ocean Turbulence Model (GOTM) [Burchard *et al.*,

1999] using a  $\kappa - \varepsilon$  turbulent scheme. Initial conditions for the 3D transport model are set to 36.5 psu and 17°C for the salinity and water temperature, respectively.

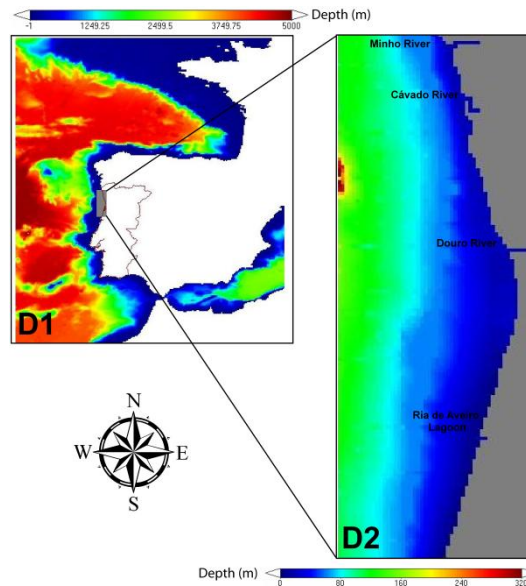


Figure 7.2: Location of the D1 and D2 domains.

The horizontal viscosity and diffusivity coefficients are set to  $2 \text{ m}^2\text{s}^{-1}$  and  $20 \text{ m}^2\text{s}^{-1}$  for D2 and D1 domains, respectively. In the same order, the time steps are 60 s and 180 s. The freshwater discharges were imposed offline (see previous section).

The meteorological forcing was not considered in this set of simulations. For this reason are not shown any results of the water temperature besides those that had been computed.

### 7.3 Results and Discussion

Model predictions for mean, extreme maximum and extreme minimum Ria de Aveiro lagoon outflows are shown in Figure 7.3, Figure 7.4, and Figure 7.5, respectively. These figures show the predictions for the following four moments: two hours after discharge peak values for spring and neap tide. As there is a phase delay between velocity and salt transport, identified as close to  $90^\circ$  between  $V(t)$  and  $S(t)$  by Vaz [2007] for the Espinheiro channel, the model predicted results are presented those two hours after each discharge peak value in order to distinguish the estuarine plume based on the salinity values.

The model predictions for mean and extreme maximum outflow scenarios correspond very well to the ideal near-field plume described by Hetland [2005] (Figure 3.1). Both simulations show an offshore bulge propagating to the open sea. Also, the predictions show salinity stratification from the lagoon mouth to the plume maximum extension. After the bulge formation, the near-field plume is advected to the right due to the Coriolis effect, extending along the northern coast due to accumulation of water in geostrophic equilibrium. These patterns suggest an approximation to the *surface-advected* plume presented by Yankovsky and Chapman [1997], (Figure 3.2).

The model predictions for the minimum river inflow scenario present a quasi-inexistent plume. In Figure 7.5 it is important to note that the scale and the reference isohaline are closer to the ocean salinity than in the other figures. The salinity differences are minimal ( $<0.5$  psu) which

can enable the control of the estuarine plume by water temperature gradients. During January the lagoon waters are colder than the ocean waters, as it is expected. Figure 7.5 C shows an intrusion of cold and less salty water below the salt ocean waters. During the summer when the lagoon waters are warmer than the ocean waters, it is expectable that with the minimum extreme river inflow (more predictable in this season) a small near-field plume will be established.

In addition to this general discussion, they were calculated, for the mean and extreme maximum discharge scenarios, the  $y_s$  (Equation 3.1) and  $h_b$  (Equation 3.2). The values introduced in the formulations are set to:  $v_i(\text{mean})=0.2114 \text{ ms}^{-1}$  and  $v_i(\text{maximum})=0.2262 \text{ ms}^{-1}$  (mean inflow velocity, based only in the negative discharge values);  $h_0=15 \text{ m}$  (it is the cell depth where the discharge was imposed);  $L=1000 \text{ m}$  (D2 domain resolution cell). The  $g'$  value was calculated according to the next formula:

$$g' = g \frac{|\rho_i - \rho_0|}{\rho_0} \quad (6.1)$$

where  $g=9.81 \text{ ms}^{-2}$ ,  $\rho_0=1026 \text{ kgm}^{-3}$  (ocean);  $\rho_i(\text{mean}) = 1024 \text{ kgm}^{-3}$ ;  $\rho_i(\text{maximum}) = 1018 \text{ kgm}^{-3}$ . In this case  $g'(\text{mean}) = 0.019 \text{ ms}^{-2}$  and  $g'(\text{maximum}) = 0.076 \text{ ms}^{-2}$ . The *Coriolis* factor,  $f$ , was calculated by:

$$f = 2\Omega \sin(\text{lat}) \quad (6.2)$$

where  $\Omega=7.269 \text{ s}^{-1}$  and  $\text{lat}=40^\circ$ . Thus,  $f = 9.3 \times 10^{-5} \text{ s}^{-1}$ .

In case of the extreme maximum discharge,  $y_s$  is calculated by  $y_s = 4.24R_{di}$  because  $v_i^2 \ll g'h_0$  (see Section 3.3). The  $y_s(\text{maximum})$  is about 49 km and  $h_b(\text{maximum})$  is 2.9 m. The maximum extension of the near-field plume in the Figure 7.4 indicates a value close to 25 km. In the case of mean lagoon outflow the  $y_s(\text{mean})$  calculated is about 25 km (Equation 3.1) and the observations show a maximum extension of ~13 km (Figure 7.5). In this evaluation it is important to note that Yankovksy and Chapman [1997] formulated these equations based on a constant inflow value which it is not the case here analyzed. This difference is expected and the value reflected the tidal effect on the Ria de Aveiro lagoon outflow.

Burger and Rossby numbers were also calculated following Equations 3.4 and 3.5, and considering  $S(\text{maximum}) = 11.5 \text{ m}$ ,  $S(\text{mean}) = 5.6 \text{ m}$ ,  $R(\text{maximum}) = 0.55$  and  $R(\text{mean}) = 2.27$ . Using the diagram depicted in Figure 3.3, these values indicate that the Ria de Aveiro lagoon near-field plume is a *surface-advected* plume. It is important to refer that the plume for the mean discharge scenario is closer to the *intermediate* plume than for the other run (see Yankovsky and Chapman [1997]).

The  $h_b$  (Equation 3.2) is an important factor to measure the equilibrium depth. This issue describes the relative importance between the density differences (buoyancy forces), the flow input and the *Coriolis* parameter. A higher input flow rate and a larger density difference between these two flows, makes the plume depth  $h_b$  (near the mouth) larger. A larger density difference means a higher buoyancy force. Then, it is easy to note that in the extreme maximum discharge scenario (with a lesser density input flow) the buoyancy force is greater than for the mean discharge. The  $h_b$  calculation ( $h_b(\text{maximum})=2.9 \text{ m}$  and  $h_b(\text{mean})=5.6 \text{ m}$ ) and the analysis of Figure 7.1C and 6.2C reveal that in this two scenarios the density gradient is more important than the mean velocity

input flux. Also, it is expectable that with a small depth, the offshore extension of the near-field plume will be greater, caused by the velocity input in this the buoyancy layer. This case is close to the two-layer classic dynamic model described in the early estuarine plumes studies [Garvine, 1987].

To post-processing the sensor TM images it was used the ArcGis® software. It was chosen an image from day 18<sup>th</sup> December 2006 as an example. The comparison between the remote sensing image and the model prediction does not pretended to reproduce a concurrent scenario and therefore the season is not fundamental. In the post-processing procedure it was created a RGB image of composite band (321 - visible) to verify the establishment of an estuarine plume. In addition, it was used the band 6 (Thermal Infrared Band) to indentify the different water temperature patterns.

This post-processing approach doesn't indicate the absolute surface temperature; only suggest different patterns in water thermal quality. With this objective, the reflectance values from Thermal Infrared Band were reclassified, using the color scale, in order to clearly distinguish the thermal properties of the mouth lagoon water into the coastal waters. Thus, Figure 7.6 shows a possible Ria de Aveiro estuarine plume during a winter period. It is evident the similarities between the predictions and the observed image. The bulge radius has about 14 km which is close to the one found for the mean discharge scenario. The inflow direction is different (NE-SW) from the predicted direction (E-W), but the northern advection alongshore is visible.

Winds direction and magnitude, before the establishment of this plume (Figure 7.6E) had some variability, despite some northern wind predominance. This can explain the higher presence of estuarine waters southern the lagoon mouth than northern. The predominant coastal current is to the north, but it is usually weak and more variable than the summer coastal current (N-S).

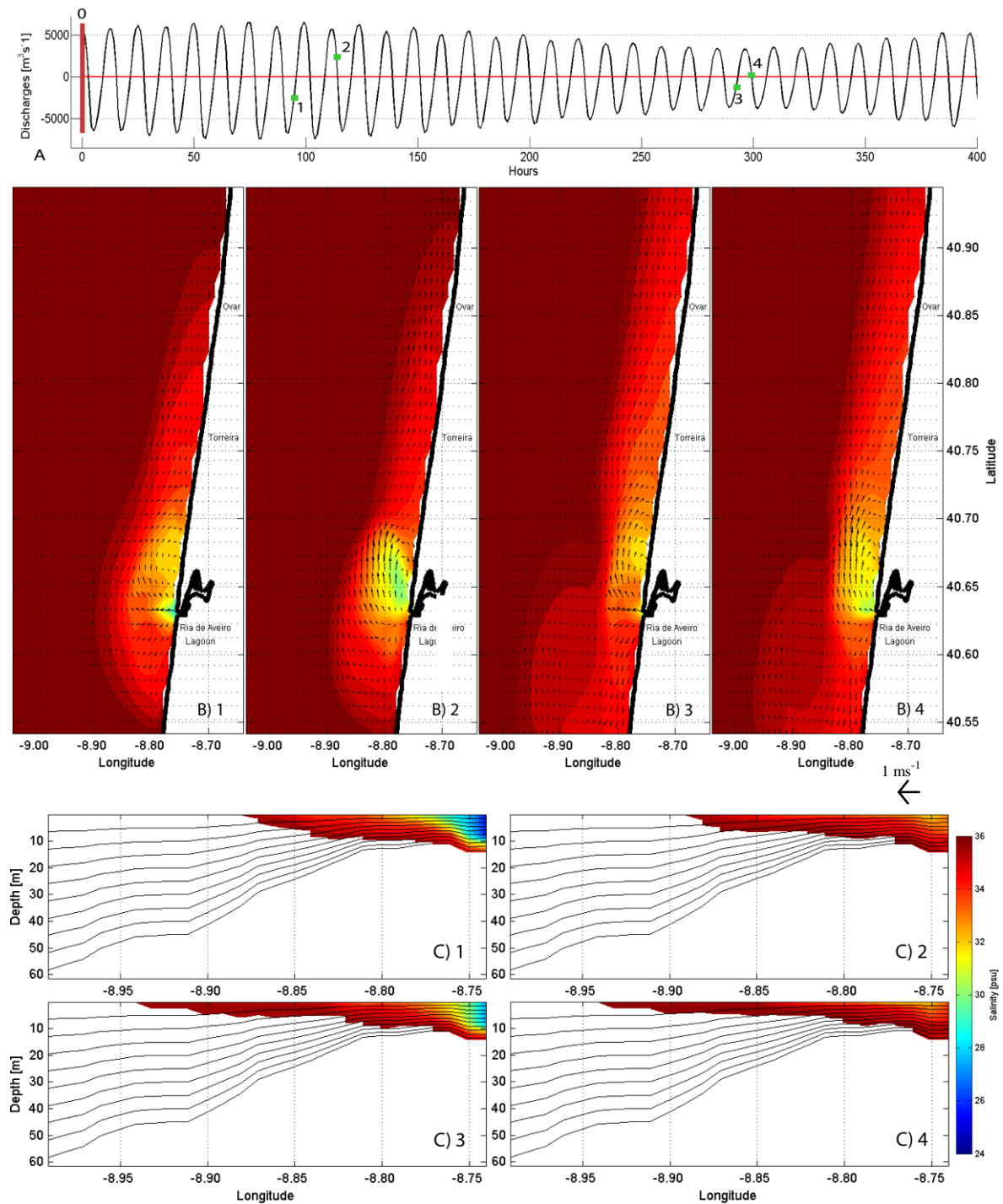


**Figure 7.3: Average discharge scenario predictions during January. A) Time series of discharge through the lagoon mouth (red line means the limit between the positive (into the lagoon) and negative (into the ocean) outflow; the green points represent the time for model outputs; 0 is the simulation initial time). B) Salinity horizontal patterns and velocity fields for each time step – 1, 2, 3, and 4. C) Salinity cross-section perpendicular to Ria de Aveiro mouth in each time step – 1, 2, 3, and 4 (salinity values above 36 psu are shown in white).**

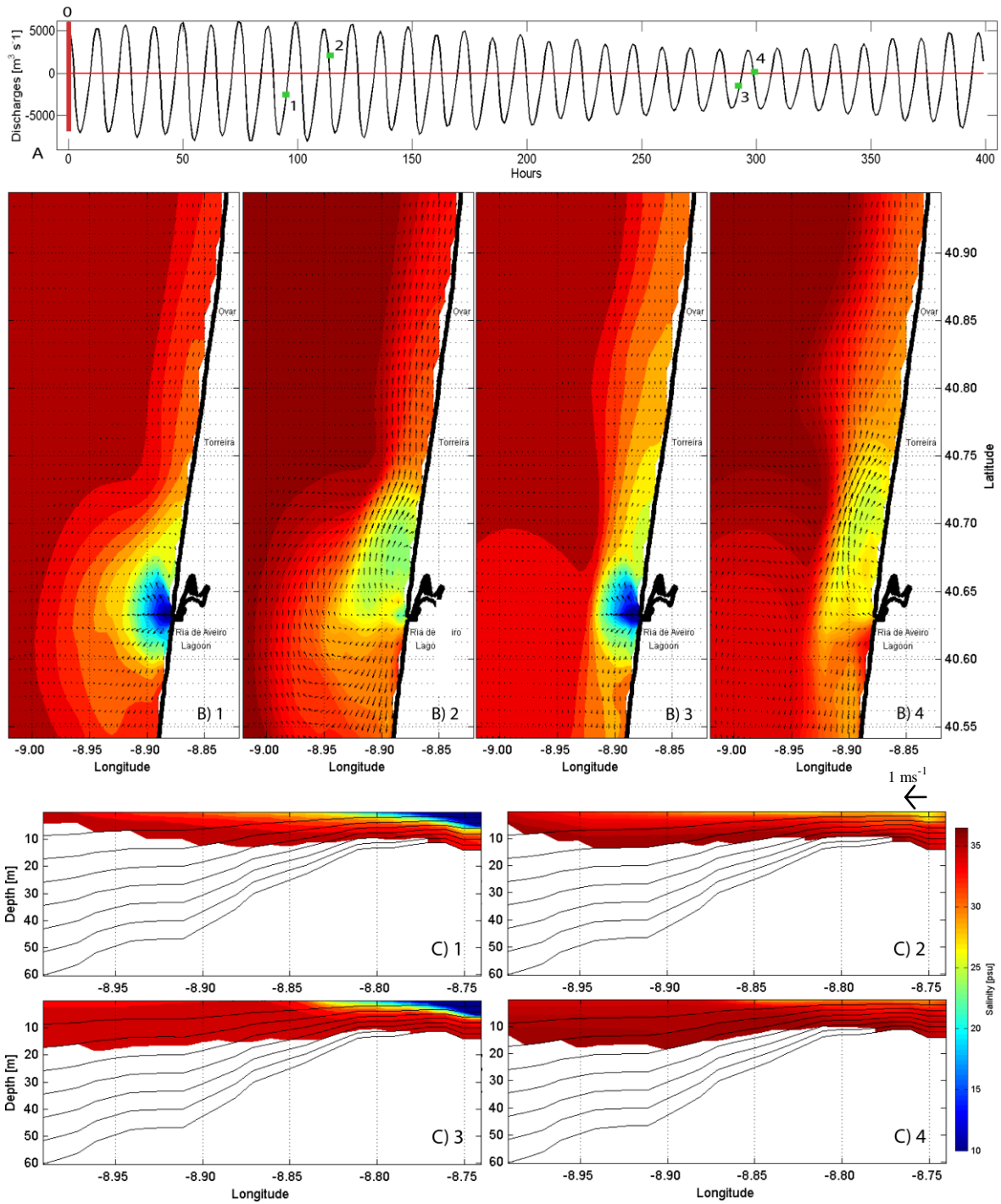


**Figure 7.4:** Extreme maximum discharge scenario predictions during January. **A)** Time series of discharge through the lagoon mouth (red line means the limit between the positive (into the lagoon) and negative (into the ocean) outflow; the green points represent the time for model outputs; 0 is the simulation initial time). **B)** Salinity horizontal patterns and velocity fields for each time step – 1, 2, 3, and 4. **C)** Salinity cross-section perpendicular to Ria de Aveiro mouth in each time step – 1, 2, 3, and 4 (salinity values above 36 psu are shown in white).

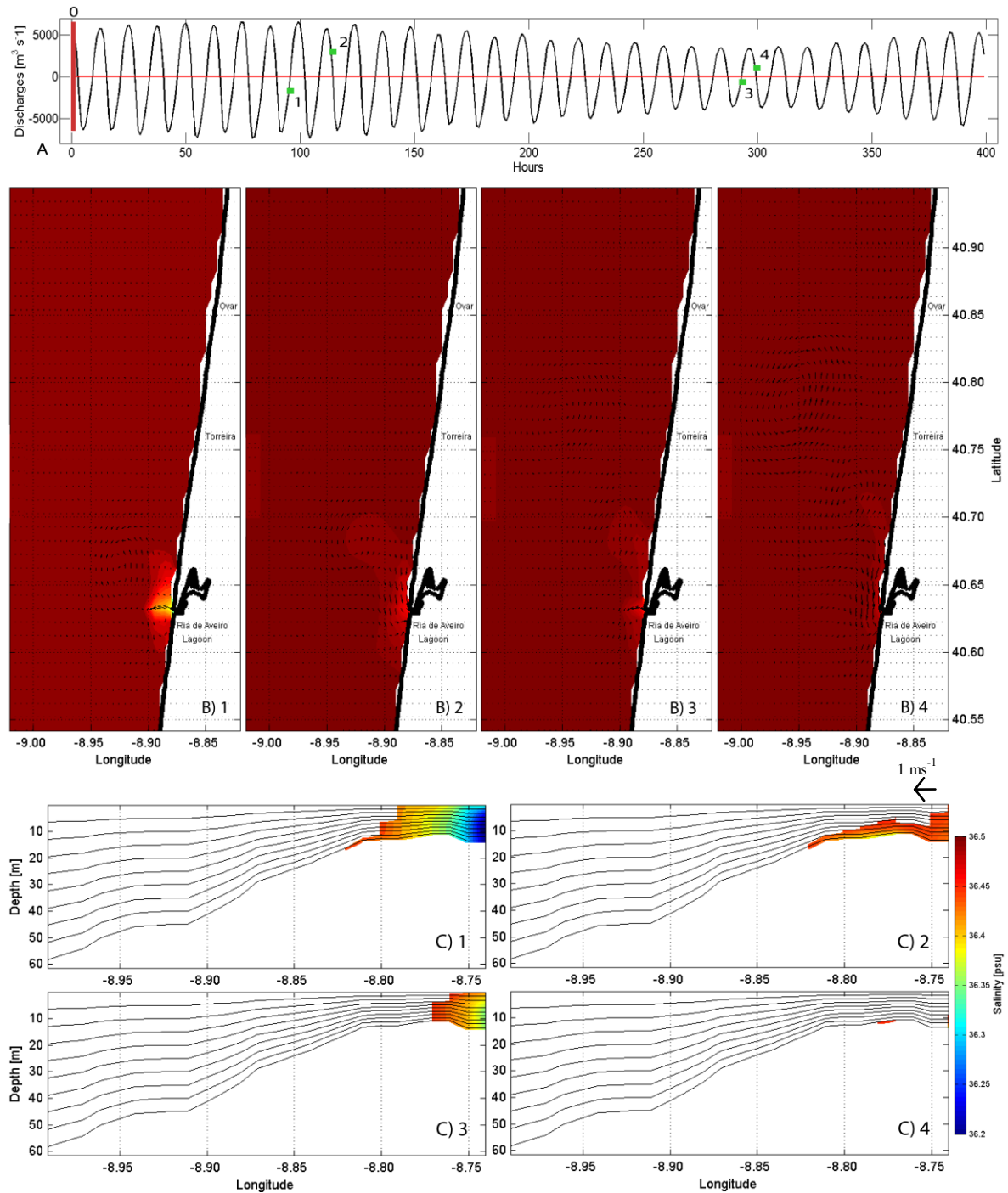


**Figure 7.5: Extreme minimum discharge scenario predictions during January. A) Time series of discharge through the lagoon mouth (red line means the limit between the positive (into the lagoon) and negative (into the ocean) outflow; the green points represent the time for model outputs; 0 is the simulation initial time). B) Salinity horizontal patterns and velocity fields for each time step – 1, 2, 3, and 4. C) Salinity cross-section perpendicular to Ria de Aveiro mouth in each time step – 1, 2, 3, and 4 (salinity values above 36 psu are shown in white).**

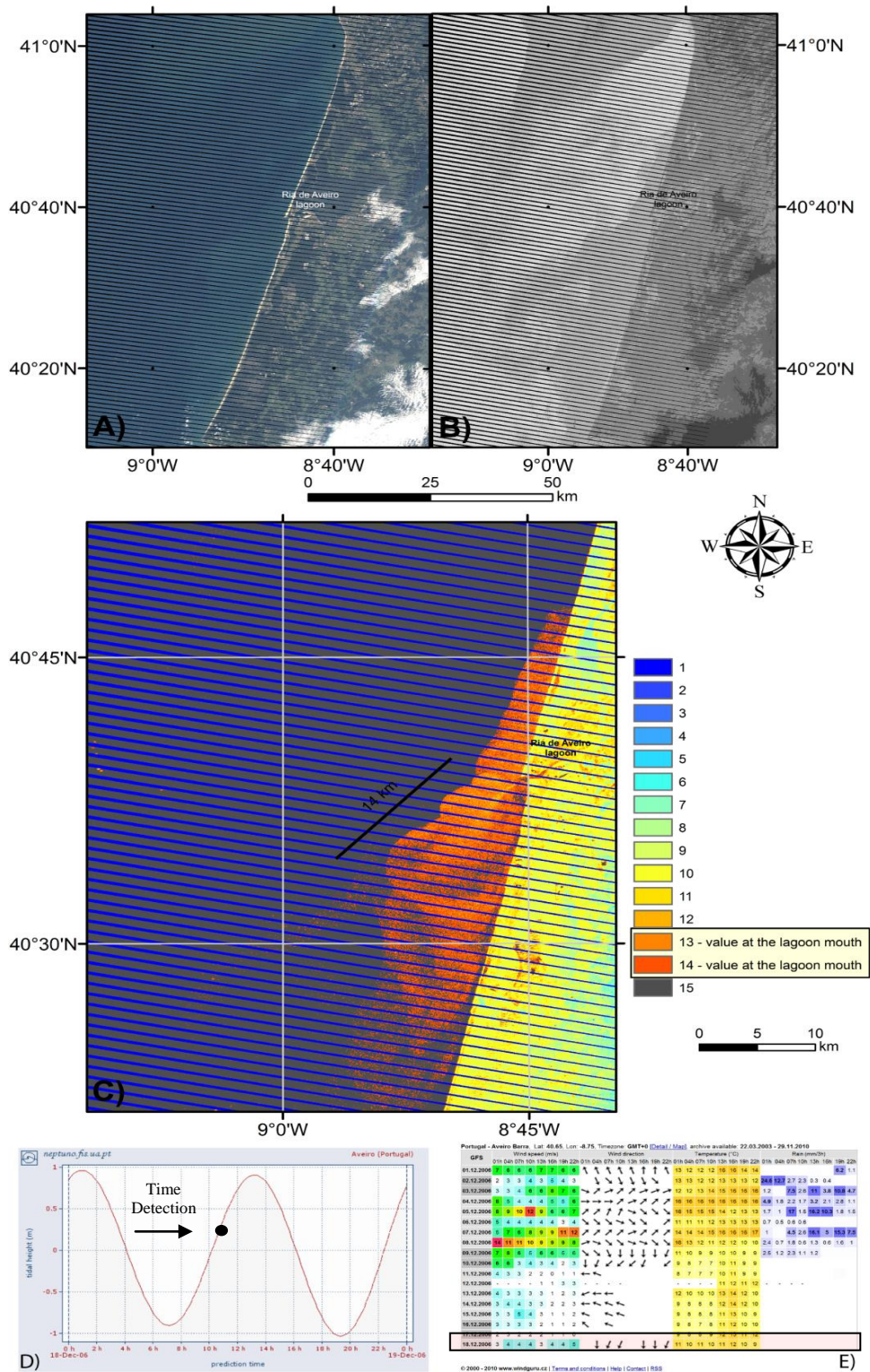


Figure 7.6: Landsat7-TM observations in 18th December 2006. A) Composite of RGB bands of TM sensor (visible image). B) Thermal Infrared Band of TM sensor. C) Reclassification of Thermal Infrared Band to distinguished the surface ocean waters with the same thermal characteristics as the lagoon mouth waters. D) Tidal prediction for Aveiro by neptuno.fis.ua [Marta-Almeida and Dubert, 2006] (11:04 was the time detection); E) Meteorological conditions computed for Aveiro by windguru.cz.



## 8 Conclusions and Future Improvements

All the proposed objectives for this work were achieved. The Mohid – 2D hydrodynamic and transport modules were implemented for Ria de Aveiro, including the construction of an actual numerical bathymetry appropriate to perform the numerical coupling with coastal models (Chapter 5). Furthermore, the use of two numerical grids demonstrated that differences in the general circulation of the Ria de Aveiro are negligible when considering the low lying coastal adjacent flooded areas, but some consistent patterns were found that suggest that the inclusion of these areas are important for more accurate studies.

The models (hydrodynamic and transport) were successfully calibrated and validated by comparing predicted and independent measured data sets.

The nested coupling between the coastal and the Ria de Aveiro models was achieved and it allowed the study of the estuarine plume formation.

It was constructed a thematic map of the Ria de Aveiro estuarine plume from remote sensing image (Section 7.3). The Ria de Aveiro of estuarine plume predicted by the Mohid 3D numerical model has a similar pattern to the plume detected in the TM-Landsat7 image. The Ria de Aveiro estuarine plume was classified as a near-field and surface-advected plume, according to the Hetland [2005] and Yankovsky and Chapman [1997] formulations. The Ria de Aveiro estuarine plume was classified as a near-field and surface-advected plume, according to the Hetland [2005] and Yankovsky and Chapman [1997] formulations. The lagoon near-field plume is characterized by a bulge near the mouth which is advected alongshore to the north due to the geostrophic equilibrium between the Coriolis and surface pressures. This circulation was found for mean and extreme maximum outflows scenarios. The plume is almost inexistent for minimum river inflows scenario. In this case the salinity differences between the lagoon and the ocean are minimal, which can induce an estuarine plume controlled by the horizontal thermal gradients.

This work constitutes a starting point for further studies and improvements in the monitoring of the dynamics of the Ria de Aveiro near-field plume. The next step of this work will be to carry out a simulation with low outflow rate, but in the summer period. From this approach it is expected to show is the establishment of a smaller estuarine plume when compared to the higher discharge scenarios.

Another improvement to perform in the future consists in linking the different outflow scenarios to different wind fields forcing. In fact, the wind forcing could play a critical role in the processes conducting to the plume establishment and induce different plume properties [Whitney and Garvine, 2005].

The coastal currents are also important in plume dynamics [Fong and Gyer, 2002]. Therefore, it is also relevant to incorporate in this model the coastal currents forcing, especially the Portugal Coastal Current and its seasonal changes (it should be used as forcing the MERCATOR Global Ocean results [Bahurel *et al.*, 2001]).

A final improvement for the estuarine plume simulation studies consists in defining accurate inputs for the river inflows and in incorporating local meteorological data (air temperature, radiation, wind fields, cloud cover, etc...) to be determined from meteorological models providing good temporal and spatial resolution values.

Thus, the Ria de Aveiro estuarine plume model (hydrodynamic and transport) could accurately calibrated and validated by remote sensing images (with more resolution and confidence

than those used in Section 7.3) comparison. The calibration and validation of this model could be improved using observed field data offshore Ria de Aveiro lagoon (if available). This approach could be more expensive than the remote sensing calibration and validation method, but will present more realistic results and may make possible the acquisition of another type of data, such as biogeochemical data.

As referred in the introduction chapter (Section 1.1), the estuarine plumes are relevant to many aspects of the coastal environment: the enhancement of biological production; the hampering of primary production; coastal pollution; larval transport; sediment and geochemical transport; etc. For these reasons, many of them linked to the socio-economic factors which are important to the populations, one of most important improvements to perform will consist in the incorporation of an ecological model (i.e. Mohid.life [Mateus, 2006]).

## References

- Abbott, M. B., Basco, D. R., 1994. *Computational Fluid Dynamics: An Introduction for Engineers*. Longman Scientific and Technical, London, 425 p.
- Arakawa, A., Lamb, V., 1977. Computational design of the basic dynamical processes of the UCLA general circulation model. *Methods in Computational Physics*, **17**, 174–267.
- Araújo, I. G. B., 2005. *Sea Level Variability: Examples from Atlantic Coast of Europe*. PhD Thesis, School of the National Oceanography Centre, Southampton, UK, 216 p.
- Araújo, I., Dias, J.M., Pugh, D., 2008. Model simulations of tidal changes in a coastal lagoon, the Ria de Aveiro (Portugal). *Continental Shelf Research*, **28**, 1010-1025.
- Avicola, G., Huq, P., 2003. The characteristics of recirculating bulge region in coastal buoyant outflows. *Journal of Marine Research*, **61**, 435 – 463.
- Baharel, P., De Mey, P., De Prada, T., Dombrowsky, E., Josse, P., Le Provost, C., Le Traon, P. Y., Piacentini, A., Siefridt, L., 2001. MERCATOR, forecasting global ocean. *AVISO Altimetry Newsletter*, **8**, 14-16.
- Bernardes, B., 2007. *Hydrodynamical and Ecological Modelling of the North Sea*. MSc dissertation thesis Technical University of Lisbon, Lisboa, Portugal, 81 p.
- Blanton, J., Amft, J., Tissue, T., 1997. Response of a small-scale bottom-attached estuarine plume to wind and tidal dissipation. *Journal of Coastal Research*, **13** (2), 349–362.
- Braunschweig, F., Martins, F., Chambel, P., Neves, R., 2003. A methodology to estimate renewal time scales in estuaries: the tagus estuary case. *Ocean Dynamics*, **53**, 137–145.
- Brock, T.D., 1981. Calculating solar radiation for ecological studies. *Ecological Modelling*, **14**, 1-19.
- Burchard, H., Bolding, K., Villarreal, M. R., 1999. *GOTM, A General Ocean Turbulence Model: Scientific Documentation*. Technical Report, European Community, Ispra, Italy.
- Chant, R. J., Wilkin, J., Zhang, W., Choi, B-J., Hunter, E., Castelao, R., Glenn, S., Jurisa, J., Schofield, O., Houghton, R., Kohut, J., Frazer, T. K., Moline, M. A., 2008. Dispersal of the Hudson River plume in the New York bight: synthesis of observational and numerical studies during LaTTE, *Oceanography*, **21.4**, 148-161.
- Chao, S. -Y., 1988. River forced estuarine plumes. *Journal of Physical Oceanography*, **18**, 2137-2149.
- Chapra, S. C., 1997. *Surface Water Quality Modeling*. Civil engineering series. McGraw-Hill. New York. 4596.
- Chen, R.F., Gardner, G.B., 2004. High-resolution measurements of chromophoric dissolved organic matter in the Mississippi and Atchafalaya River plume regions. *Marine Chemistry*, **89** (1–4), 103–125.
- Cheng R.T., Burau J.R., Gartner, J.W., 1991. Interfacing data analysis and numerical modelling for tidal hydrodynamic phenomena. In: B.B. Parker, Editor, *Tidal Hydrodynamics*, John Wiley & Sons, New York, USA (1991), pp. 201–219.
- Choi, B.J. and Wilkin, J.L., 2006. The effect of wind on the dispersal of the Hudson River plume. *Journal of Physical Oceanography*, **37**, 1878-1897.

- Coelho, H., Neves, R., White, M., Leitão, P., Santos, A., 2002. A Model for Ocean Circulation on the Iberian Coast. *Journal of Marine Systems*, **32(1-3)**, 153-179.
- Dias J.M., Lopes J.F., 2006. Implementation and assessment of hydrodynamic, salt and heat transport models: The case of Ria de Aveiro lagoon (Portugal). *Environmental Modelling & Software*, **21**, 1-15.
- Dias J.M., Sousa M., Bertin X., Fortunato A., Oliveira A., 2009. Numerical modeling of the impact of the Ancão inlet relocation (Ria Formosa, Portugal). *Environmental Modelling & Software*, **24**, 711-725.
- Dias, J. M., 2001. *Contribution to the Study of the Ria de Aveiro Hydrodynamics*. PhD thesis, University of Aveiro, Portugal, 288 p.
- Dias, J. M., Fernandes, E. H., 2006. Tidal and subtidal propagation in two atlantic estuaries: Patos lagoon (Brazil) and Ria de Aveiro lagoon (Portugal). *Journal of Coastal Research*, **SI 39**, 1422 – 1426.
- Dias, J.M., Lopes, J.F., Dekeyser, I., 1999. Hydrological characterisation of Ria de Aveiro, Portugal, in early Summer. *Oceanologica Acta*, **22**, 473–485.
- Dias, J.M., Lopes, J.F., Dekeyser, I., 2000. Tidal propagation in Ria de Aveiro Lagoon, Portugal. *Physics and Chemistry of the Earth (B)*, **25 (4)**, 369-374.
- Fichez, R., Jickells, T.D., Edmunds, H.M., 1992. Algal blooms in high turbidity, a result of the conflicting consequences of turbulence on nutrient cycling in a shallow water estuary. *Estuarine, Coastal and Shelf Science*, **35**, 577–593.
- Fong, D. A., Geyer, W. R., 2001. Response of a river plume during an upwelling favorable wind event. *Journal of Geophysical Research*, **106**, 1067–1084.
- Fong, D.A., Geyer, W.R., 2002. The alongshore transport of freshwater in a surface-trapped river plume. *Journal of Physical Oceanography*, **32**, 957 – 972.
- Frazão O., Pereira D., Santos J.L., Dias I., Dias J.M., Vaz N., Teixeira M., Quintela A., Ferreira J., Ferreira L.A., Araújo F.M., 2010. Industrialization of advanced optical technologies for environmental monitoring. *Clean Technologies and Environmental Policy*. **12**, 65-73.
- Froidefond, J.M., Jegou, A.M., Hermida, J., Lazure, P., Castaing, P., 1998. Variability of the Gironde turbid plume by remote sensing. Effects of climatic factors. *Oceanologica Acta*, **21**, 191–207.
- García Berdeal, I., Hickey, B. M. Kawase, M., 2002. Influence of wind stress and ambient flow on a high discharge river plume. *Journal of Geophysical Research*, **107**, 3130.
- Garvine, R. 1987. Estuary plumes and fronts in shelf waters: A layer model. *Journal of Physical Oceanography*, **17:1**,877–1,896.
- Génio L., Sousa A., Vaz N., Dias J.M., Barroso C.M., 2008. Effect of low salinity on the survival of recently hatched veliger of *Nassarius reticulatus* (L.) in estuarine habitats: a case study of Ria de Aveiro. *Journal of Sea Research*, **59, 3**, 133-143
- Guo, X., Valle-Levinson, A., 2007. Tidal effects on estuarine circulation and outflow plume in the Chesapeake Bay. *Continental Shelf Research*, **27**, 20-42.
- Halverson, M. J., Pawlowicz, R., 2008. Estuarine forcing of a river plume by river flow and tides, *Journal of Geophysical Research*, **113**, C09033
- Hetland, R. D., 2005. Water mass structure of wind forced river plumes, *Journal of Physical Oceanography*, **35(9)**, 1667-1688.

- Horner-Devine, A.R., Fong, D.A., Monismith, S.G., Maxworthy, T., 2006. Laboratory experiments simulating a coastal river outflow. *Journal of Fluid Mechanics*, **555**, 203–232.
- Hsu, M.H. and A.Y. Kuo, J.T. Kuo and W.C. Liu. 1999. Procedure to calibrate and verify numerical models of estuarine hydrodynamics. *ASCE Journal of Hydraulic Engineering*, **125** (2): 166-182.
- IPCC, 2007. *Climate Change 2007: The Physical Science Basis. Contribution of the Working Group I to the Fourth Assessment Report of the Intergovernmental Panel on Climate Change* [Solomon, S., Qin, D., Manning M., Chen, Z., Marquis M., Averyt K.B., Tignor M., Miller H.L. (eds.)]. Cambridge University Press, Cambridge, United Kingdom and New York, USA, 996 pp.
- Janzen, C. D., Wong, K.-C., 2002. Wind-forced dynamics at the estuary-shelf interface of a large coastal plain estuary. *Journal of Geophysical Research*, **107**, 3138.
- Jerlov, N. G., 1968. *Optical Oceanography*. American Elsevier Publication, New York. 194p.
- Jouanneau, J.M., Latouche, C., 1982. Estimation of fluxes to the ocean from mega-tidal estuaries under moderate climates and the problems they present. *Hydrobiologia*, **91**, 23–29.
- Kraus, E. B., 1972. *Atmosphere-Ocean Interaction*. Clarendon Press, Oxford, 275 pp.
- Le Pape, O., Chauvet, F., Desaunay, Y., Guéralut, D., 2003. Relationship between the interannual variations of the river plume and the extent of the nursery grounds for the common sole (*Solea solea*, L.) in Villaine Bay. Effects on recruitment variability. *Journal of Sea Research*, **50**, 177–185.
- Leendertse, J., 1967. *Aspects of a Computational Model for Long Water Wave Propagation*. Memorandum rh-5299-rr, Rand Corporation, Santa Monica, 165 p.
- Leendertse, J., Liu, S., 1978. A three-dimensional turbulent energy model for non-homogeneous estuaries and coastal sea systems. In: Nihoul, J. (Ed.), *Hydrodynamics of estuaries and Fjords*. Elsevier, Amsterdam, 387–405.
- Leitão, P. C., 2003. *Integração de Escalas e de Processos na Modelação do Ambiente Marinho*. PhD thesis Instituto Superior Técnico. Universidade Técnica de Lisboa, Lisboa, Portugal, 296p.
- Leitão, P., Coelho, H., Santos, A., Neves, R., 2005. Modelling the main features of the Algarve coastal circulation during July 2004: A downscaling approach. *Journal of Atmospheric and Ocean Science*, **10** (4), 421–462.
- Li, M., L. Zhong, and W. C. Boicourt. 2005. Simulations of Chesapeake Bay estuary: Sensitivity to turbulence mixing parameterizations and comparison with observations, *Journal of Geophysical Research*, **110**, C12004.
- Lihan, T., Saitoh, S.I., Iida, T., Hirawake, T., Iida, K., 2008. Satellite-measured temporal and spatial variability of the Tokachi River plume. *Estuarine, Coastal and Shelf Science*, **78**, 237-249.
- Lyard, F., Lefevre, F., Letellier, T., Francis, O., 2006. Modelling the global ocean tides: modern insights from fes2004. *Ocean Dynamics*, **56**, 5-6, 394-415.
- Malhadas MS, Silva A, Leitão PC, Neves R, 2009. Effect of the Bathymetric Changes on the Hydrodynamic and Residence Time in Óbidos Lagoon (Portugal). *Journal of Coastal Research*, Lisbon, Portugal, **56**, 549 - 553.

- Marsaleix, P., Estournel, C., Kondrachoff, V., Vehil, R., 1998. A numerical study of the formation of the Rhone River plume. *Journal of Marine Systems*, **14**, 99–115.
- Marta-Almeida, M. and Dubert, J., 2006. The structure of tides in the Western Iberian region. *Continental Shelf Research*, **26**, 385-400.
- Martins, F., Leitão, P., Silva, A., Neves, R., 2001. 3D modelling in the Sado estuary using a new generic vertical discretization approach. *Oceanologica Acta*, **24 (1)**, 1–12.
- Mateus, M., 2006. *A Process-oriented Biogeochemical Model for Marine Ecosystems: Development, Numerical Study, and Application*. PhD Thesis. IST, Lisboa.
- Mendes, R., Dias, J.M., Pinheiro, L.M., 2009. Numerical modeling estimation of the spread of maritime oil spills in Ria de Aveiro lagoon. *Journal of Coastal Research*. **SI56**, 1375-1379, 252p.
- Mendes, R., Vaz, N., Dias, J.M., *submitted*. Numerical modeling changes induced by the low lying areas adjacent to Ria de Aveiro. *Journal Coastal Research*.
- Mestres, M., Sierra, J.P., Sánchez-Arcilla, A., 2007. Factors influencing the spreading of a low-discharge river plume. *Continental Shelf Research*, **27**, 2116–2134.
- Montero, P., 1999. *Estudio de la Hidrodinámica de la Ría de Vigo Mediante un Modelo de Volúmenes Finitos*. Ph.D. thesis, Universidad de Santiago de Compostela, Spain, 174 p.
- Moreira, M. H., Queiroga, H., Machado, M. M., Cunha, M. R., 1993. Environmental gradients in a southern estuarine system: Ria de Aveiro, Portugal, implication for soft bottom macrofauna colonization. *Netherland Journal of Aquatic Ecology*, **27 (2-4)**, 465–482.
- Morris, A.W., Allen, J.I., Howland, R.J., Wood, R.G., 1995. The estuary plume zone: source or sink of land-derived nutrient discharges? *Estuarine, Coastal and Shelf Science*, **40**, 387–402.
- Naudin, J.J., Cauwet, G., Fajon, C., Oriol, L., Terzić, S., Devenon J.L., Broche, P., 2001. Effect of mixing on microtidal communities in the Rhône River plume. *Journal of Marine Systems*, **28 (3-4)**, 203–227
- Orton, P.M. and Jay, D.A., 2005. Observations at the tidal plume front of a high-volume river outflow. *Geophysical Research Letters*, **32**, L11605.
- Otero, P., Ruiz-Villarreal, M., Peliz, A., Cabanas, J.M., 2010. Climatology and reconstruction of runoff time series in Northwest Iberia: influence in the shelf buoyancy budget. *Scientia Marina*, **74 (2)**, 247.
- Paulson, C. A., Simpson, J. J., 1977. Irradiance measurements in the upper ocean. *Journal of Physical Oceanography*, **7**, 952–956.
- Pawlowicz, R., Beardsley, B., Lentz, S., 2002. Classical tidal harmonic analysis including error estimates in MATLAB using T TIDE. *Computers and Geosciences*, **28**, 929–937.
- Picado, A., Dias, J.M., Fortunato, A. B., 2010. Tidal changes in estuarine systems induced by local geomorphologic modifications. *Continental Shelf Research*, **30**, 17, 1854-1864.
- Pugh, D.T., 1996. *Tides, Surges and Mean Sea-Level* (reprinted with corrections). John Wiley & Sons Ltd, Chichester, UK, 486 pp.
- Pullen, J. D., Allen, J. S., 2000. Modeling studies of the coastal circulation off northern California: shelf response to a major Eel River flood event. *Continental Shelf Research*, **20**, 2213–2238.

- Ribeiro, A.C., Peliz Á., Santos, A.M.P., 2005. A study of the response of the chlorophyll-a biomass to a winter upwelling event off Western Iberia using SeaWiFS and in situ data, *Journal of Marine Systems*, **53**, pp. 87–107
- Santos, A. J. P., 1995. *Modelo Hidrodinâmico Tridimensional de Circulação Oceânica e Estuarina*. PhD Thesis, Universidade Técnica de Lisboa, Lisboa, 273 p.
- Santos, A.M.P., Peliz, Á., Dubert, J., Oliveira, P.B., Angélico, M.M., Ré, P., 2004. Impact of a winter upwelling event on the distribution and transport of sardine (*Sardina pichardus*) eggs and larvae off Western Iberia: a retention mechanism, *Continental Shelf Research*, **24** (2), 149–165
- Santos, M., Neves, R., Leitão, P., Pereira, P., Pablo, H., Fernandes, L. D., Carvalho, S. M., Alves, C. P., 2006. *Qualidade da água da Lagoa de Óbidos: Que futuro?* XII Encontro Nacional de Saneamento Básico, Cascais 2006.
- Saraiva, S, Pina, P, Martins, F., Santos, M., Braunschweig, F., Neves, R., 2007. Modelling the influence of nutrient loads on Portuguese estuaries. *Hydrobiologia*, **587**, 5–18.
- Silva, A., 1996. *Implementação de um Modelo Hidromorfológico para a Barra do Douro Contribuição para a Compreensão do Sistema*. 3º Congresso da Água, Lisboa.
- Silva, A.J.R., Leitão, P.C., Leitão, J.C., Braunschweig, F., Neves, R., 2002. Ria Formosa 3D hydrodynamic model. A contribution for the understanding of the Faro Olhão inlet processes. *Litoral 2002, The Changing Coast. EUROCOAST, Portugal*, 197–207.
- Swinbank, W. C., 1963. Long-wave radiation from clear skies. *Quarterly Journal of the Royal Meteorological Society*, **89**, 339–348.
- Taboada, J. J., Prego, R., Ruiz-Villarreal, M., Montero, P., Gómez-Gesteira, M., Santos, A., Pérez Villar, V., 1998. Evaluation of the seasonal variation in the residual patterns in the Ría de Vigo (NW Spain) by means of a 3D baroclinic model. *Estuarine, Coastal and Shelf Science*, **47**, 661–670.
- Teixeira, S., 1994. *Dinâmica Morfossedimentar da Ria de Aveiro (Portugal)*. PhD Thesis. Faculdade de Ciências da Universidade de Lisboa, Portugal, 397 p.
- Trancoso, A.R., Saraiva, S., Fernandes, L., 2005. Modelling macroalgae using a 3D hydrodynamic-ecological model in a shallow, temperate estuary. *Ecological Modelling*, **187**, 232-246.
- Vaz N., Dias J.M., Leitão P.C., 2009a. Three-dimensional modelling of a tidal channel: the Espinheiro Channel (Portugal). *Continental Shelf Research*, **29**, 29-41.
- Vaz, N., Dias, J. M., Leitão, P., Martins, I., 2005. Horizontal patterns of water temperature and salinity in an estuarine tidal channel: Ria de Aveiro. *Ocean Dynamics*, **55**, 416–429.
- Vaz, N., Dias, J.M., Leitão, P.C., Nolasco, R., 2007. Application of the Mohid-2D model to a mesotidal temperate coastal lagoon. *Computers & Geosciences*, **33**, 1204-1209.
- Vaz, N., Fernandes, L., Leitão, P.C., Dias, J.M., Neves, R., 2009b The Tagus estuarine plume induced by wind and river runoff: Winter 2007 case study. *Journal of Coastal Research*, **SI56**, 1090-1094.
- Vaz, N.A.F., 2007. *Study of Heat and Salt Transport Processes in the Espinheiro Channel (Ria de Aveiro)*. Phd thesis, Universidade de Aveiro, Aveiro, Portugal, 151 pp.
- Villarreal, M. R., Montero, P., Taboada, J. J., Prego, R., Leitão, P. C., Pérez-Villar, V., 2002. Hydrodynamic model study of the Ria de Pontevedra under estuarine conditions. *Estuarine, Coastal and Shelf Science*, **54** (1), 101–113.

- 
- Villarreal, M., Coelho, H., Díaz del Río, G., Nogueira, J., 2004. Slope current in the Cantabrian: observations and modeling of seasonal variability and interaction with Aviles Canyon. *1st EGU General Assembly*, France.
  - Warner, J. C., Geyer, W. R., Lerczak, J. A., 2005. Numerical modelling of an estuary: a comprehensive skill assessment. *Journal of Geophysical Research*, **110**, C05001.
  - Weaver, A.J., Hsieh, W.W., 1987. The influence of buoyancy flux from estuaries on continental shelf circulation, *Journal of Physical Oceanography*, **17**, 2127–2140.
  - Whitney, M. M., Garvine, R. W., 2005. Wind influence on a coastal buoyant outflow. *Journal of Geophysical Research*, **110**, C03014.
  - Wilmott, C.J., 1981. On the validation of models. *Physical Geography*, **2**, 184–194.
  - Xu, Z., 2000. *Ellipse Parameters Conversion and Vertical Velocity Profiles for Tidal Currents*. Maurice-Lamontagne Institute. Ocean Science Division, Fisheries and Oceans, Canada, 24p.
  - Yankovsky, A., Chapman, D.C., 1997. A simple theory for the fate of buoyant coastal discharges. *Journal of Physical Oceanography*, **27**, 1386–1401.